NASA MEMO 10-29-58L

NASA

MEMORANDUM

EFFECT OF SEVERAL AFTERBODY MODIFICATIONS INCLUDING TERMINAL FAIRINGS ON THE DRAG OF A SINGLE-ENGINE FIGHTER MODEL WITH HOT-JET EXHAUST

By John M. Swihart, Harry T. Norton, Jr.,
and James W. Schmeer

Langley Research Center
Langley Field, Va.

NATIONAL AERONAUTICS AND SPACE ADMINISTRATION

WASHINGTON

December 1958

NATIONAL AERONAUTICS AND SPACE ADMINISTRATION

MEMORANDUM 10-29-58L

EFFECT OF SEVERAL AFTERBODY MODIFICATIONS INCLUDING TERMINAL FAIRINGS ON THE DRAG OF A SINGLE-ENGINE FIGHTER MODEL WITH HOT-JET EXHAUST*

By John M. Swihart, Harry T. Norton, Jr.,
and James W. Schmeer

SUMMARY

An investigation of the drag characteristics of several boattailed afterbodies and afterbody terminal fairings has been conducted in the Langley 16-foot transonic tunnel utilizing a single-engine fighter model with a hot-jet exhaust. The tests were made over a Mach number range from 0.80 to 1.10 at jet total-pressure ratios up to 9. The turbojet exhaust was simulated with a hydrogen peroxide gas generator at a total temperature of about 1,350° F.

The results of the investigation indicate that the drag of these complex airplane configurations (without terminal fairings) follow the same trends as simple boattailed bodies of revolution; however, the interference effects of aerodynamic surfaces and protuberances can be large. It was also indicated that one type of afterbody terminal fairing which consisted of 8 bodies designed to improve the afterbody fineness ratio, to eliminate the excess base area, and to provide forward sloping surfaces for the underexpanded jet to act upon, reduced the drag below that of the best boattailed afterbody over most of the Mach number range of the investigation.

INTRODUCTION

Many investigations have been conducted in recent years on the effect of the jet exhaust on afterbody drag. (For example, see refs. 1 to 6.) These investigations have all served to define the cause and to offer some solutions for the drag problem due to jet interference. Reference 6 presented pressure distributions and external pressure drag

*Title, Unclassified.

[redacted]

coefficients for a series of afterbodies on a single-engine fighter model. One purpose of the present paper is to present the force and moment data for most of those afterbody configurations. An additional purpose is to show the drag coefficients and present a brief design analysis for afterbody modifications called terminal fairings. These terminal fairings, or small bodies applied externally to the basic afterbody, are designed to utilize the present knowledge of jet interference to reduce the afterbody drag and to improve the airplane performance. Some preliminary results of an application of the afterbody terminal-fairing idea are given in reference 7.

The Mach number range of the investigation was from 0.80 to 1.10 and the average Reynolds number based on wing mean aerodynamic chord was 5×10^6. A hydrogen peroxide turbojet engine simulator (ref. 8) was used to provide the hot-jet exhaust. The angle-of-attack range was from 0° to 5° but only the data for an angle of attack of 0° are reported herein.

SYMBOLS

All force and moment coefficients reported herein are for the fuselage-tail combination in the presence of the wing and are based on wing area but do not include the wing forces and moments.

A	area
AR	aspect ratio
b	wing span
C_D	drag coefficient, D/qS
C_L	lift coefficient, L/qS
C_m	pitching-moment coefficient, $M/qS\bar{c}$
C_p	pressure coefficient, $\frac{p_{local} - p_\infty}{q}$
c	local chord
$\bar{c}$	wing mean aerodynamic chord
c_r	root chord

c_t	tip chord
D	drag
d	diameter
H_2O_2	hydrogen peroxide (90 percent concentration by weight)
i_t	incidence angle of horizontal tail, relative to fuselage center line
L	lift
l	distance from plane of base, positive downstream
M	Mach number or pitching moment referred to $0.25\bar{c}$
p	absolute pressure
$p_{t,j}/p_\infty$	ratio of jet total pressure to free-stream static pressure
q	dynamic pressure
S	wing area, includes area blanketed by fuselage
$\frac{w_s}{w_p}\sqrt{\frac{T_s}{T_p}}$	corrected secondary-to-primary weight-flow ratio
β	boattail angle measured in planes normal to plane of base (see fig. 3)
ϕ	fuselage meridian angle
Λ	angle of sweep

Subscripts:

b	base
i	internal
j	jet
e	exit
∞	free-stream conditions

[redacted]

bal	measured by balance
p	primary
s	secondary
1,2,3	axial stations

APPARATUS AND METHODS

Tunnel and Support System

The investigation was conducted in the Langley 16-foot transonic tunnel which is a single-return atmospheric wind tunnel with air exchange and an octagonal slotted-throat test section. The bifurcate-sting support system used with this model is shown in figures 1 and 2 and is described in reference 6.

Model

The single-engine turbojet fighter model used for this investigation was the same model described in reference 6. Figure 1 is a sketch which gives the general dimensions of the model and support system. Figure 2 shows photographs of the single-engine fighter model installed in the Langley 16-foot transonic tunnel test section. Figure 3 shows sketches of afterbodies A, B, and D of reference 6 and gives details of the engine-ejector arrangements used in the models. Photographs of the three afterbodies and the three types of afterbody terminal fairings are shown in figure 4. Sketches of the three types of terminal fairings with typical cross sections and dimensions are shown in figure 5. The type I fairings were fitted on afterbody A, the type II and III fairings, on afterbody B. Table I gives detailed dimensions for the type I terminal fairings. An appendix is included in the paper which gives the design principles for the type I terminal fairings.

The type II terminal fairings consist of five bodies placed symmetrically about the fuselage vertical center line. They were designed to fit afterbody B with the skeg (tail hook and bumper fairing) in place. These bodies were designed subsequent to the type I fairings and were designed primarily to obtain beneficial supersonic interference. It was reasoned that the positive pressure field created by the upstream portion of the terminal bodies would create beneficial interference on the afterbody and in the base region. No particular attempt was made to secure beneficial jet interference or thrust forces on the terminal bodies themselves. The type III terminal fairings are actually five

[redacted]

sets of auxiliary air inlets which exhaust air into the base region. They have the same general design objective as the type II fairings and are also attached to afterbody B. It was estimated that beneficial interference effects would be obtained on the afterbody between the fairings at supersonic speeds. The objective of taking air into the fairings was to see whether this air would recover pressure along the converging afterbody and thereby reduce the afterbody and base drag.

Figure 6 is a cutaway view of the model showing the location of the six-component strain-gage balance and the thrust balance. The wing was rigidly attached to the support system and the fuselage-tail combination was mounted to the six-component balance supported by the wing. Flexible diaphragm seals were used at the juncture between the wing and the fuselage. The hydrogen peroxide turbojet simulator was supported from the wing in such a manner that the external drag was measured separately from the thrust. The details of these two systems have been described in reference 9.

Turbojet Simulator

A hydrogen peroxide turbojet engine simulator with a convergent nozzle and ejector was mounted in the model as shown in figures 1 and 6, and the convergent nozzle and ejector was a 1/7.5-scale model of the exit of engine B of reference 8. Complete details of the operation and the characteristics of the hydrogen peroxide turbojet engine simulator are given in reference 8.

Tests

The model was investigated over the Mach number range from 0.80 to 1.10 at 0° angle of attack. The average Reynolds number based on $\bar{c}$ was about 5×10^6 for this Mach number range. All configurations were tested at nonafterburning cruise operating conditions; some were investigated with the primary nozzle opened to afterburner position and at angle of attack; however, only the 0° angle of attack nonafterburner conditions are reported herein. Jet-on data were taken at primary jet total-pressure ratios $p_{t,j}/p_\infty$ of 2, 3, 4, 5, 7, and sometimes 9.

Secondary air was supplied to the ejector through a small nose inlet. Figure 7 shows the variation of the corrected secondary weight-flow ratio with primary total-pressure ratio for afterbodies A, B, and D at all Mach numbers. Inasmuch as the same nose inlet and engine ejector combinations were used with the terminal fairings, the same variations apply as for the basic afterbodies.

Instrumentation

Fuselage-tail forces and moments were obtained on the six-component strain-gage balance. Pressures were measured on the afterbodies, bases, in the primary and secondary exits, secondary inlet, and inside the model. Temperatures were also measured in the primary jet and the secondary system. Table II lists the locations of the pressure orifices on afterbody A with type I terminal fairings and on afterbody B with the type II and III terminal fairings for which data are presented in this paper. The pressure tubing from these orifices was conducted out of the model through the wing and support booms to a pressure transducer manifold such as is described in reference 9.

Data Reduction

The electrical signals from the strain-gage balances and the electrical pressure transducers were transmitted to carrier amplifiers and then to recording oscillographs located in the tunnel control room. The trace deflections on the recorder film were converted to forces, moments, pressures, and temperatures by machine computation. The forces, moments, and pressures were then converted to standard coefficients by machine computation. References 6 and 9 describe the technique for obtaining simultaneous force and pressure data while the jet is operating.

The cutaway view of the model shown in figure 6 outlines the drag system of the model. The external drag of the fuselage-tail combination is defined as follows:

$$D = D_{bal} + (p_i - p_\infty)\left[A_2 - \frac{1}{2}(A_2 - A_1)\right] - (p_b - p_\infty)\left[\frac{1}{2}(A_2 + A_1) - A_e\right]$$

Figure 6(b) shows the location of the pressure measurements and areas used in the equation. No measurements of the thrust forces are reported in this paper since the thrust balance was inoperative for most of the terminal-fairing investigation.

Accuracy

The following is the estimated accuracy of the data presented in this paper:

M	± 0.005
C_D	± 0.0015

C_L	±0.005
C_m	±0.001
C_p	±0.01
$p_{t,j}/p_\infty$	±0.2
$\frac{w_s\sqrt{T_s}}{w_p\sqrt{T_p}}$	±0.01

RESULTS AND DISCUSSION

Basic Aerodynamic Coefficients

The variation of the basic aerodynamic coefficients C_D, C_L, and C_m with jet total-pressure ratio $p_{t,j}/p_\infty$ is shown in figures 8 and 9 for afterbodies A, B, and D, and the three types of terminal fairings. The drag-coefficient data generally indicate the familiar trend with increasing pressure ratio; namely, a slight decrease in C_D to a pressure ratio of about 2, followed by an increase in C_D until near a pressure ratio of 4 or 5, and then another decrease with further increases in pressure ratio. Comparison of the data in figure 8(a) with the afterbody pressure drag coefficients presented in reference 6 indicates that the increments in drag coefficients between the various fuselage combinations are approximately the same as the increments between the various afterbodies which were shown in reference 6.

It is noted that the effect of jet pressure ratio on the drag coefficient of the type I terminal fairings does not show the familiar trend indicated previously. The jet appears to have a beneficial effect on the drag coefficient for pressure ratios up to about 5 at the subsonic Mach numbers. This beneficial interference effect will be shown later to have a significant effect on the afterbody drag performance at typical engine operating pressure ratios.

Pressure Coefficient Data

Figure 10 shows the variation of pressure coefficient over the afterbodies, and various surfaces of the terminal fairings at several values of jet total-pressure ratio, and two Mach numbers. Note that the zero axes on the ordinate are shifted for each nominal value of jet pressure ratio, and care should be exercised in reading the curves. The data with the terminal fairings in place are compared with the basic afterbody to detail the pressure field changes on the afterbodies due

to jet interference and the interference fields of the terminal fairings. The pressure-coefficient data will be discussed in more detail in an analysis of the drag results of the various afterbodies to be presented subsequently in this paper.

Drag Performance of Various Configurations

Conventional afterbodies.- Figure 11 shows the effect of Mach number on the drag coefficients of afterbodies A, B, and D, and the three types of terminal fairings for constant values of jet total-pressure ratio. The data indicate that afterbody D has the lowest fuselage-tail drag coefficient for the conventional afterbodies over most of the Mach number range at most values of jet total-pressure ratio. The lower drag coefficients for afterbody D are an indication that the drag of these airplane configurations (without terminal fairings) follow the same trends as simple bodies of revolution (ref. 3). The similarity of the drag coefficients for afterbodies A and B, in spite of a large difference in boattail angle, is an indication that the interference effects of aerodynamic surfaces and protuberances must be considered in the design of the afterbody shape. The foregoing conclusions were noted in reference 6 and the data presented herein have served to substantiate those conclusions.

Terminal fairing configurations.- The data of figure 11(b) indicate that the type I terminal fairings, designed to improve the afterbody fineness ratio, eliminate excess base area, and provide forward sloping surfaces for the underexpanded jet to act upon (see appendix) generally has the lowest drag coefficient of any of the terminal fairing types. A clear-cut reason for the general superiority of the type I terminal fairings cannot be given because of differences in the afterbodies to which the terminal fairings were applied, to presence of skeg on afterbody B (see ref. 6), and to the difficulty of checking the force data on these very complex configurations by integration of the local pressures. Examination of the pressure coefficients presented in figures 10(a) to 10(d), however, shows that a more positive pressure coefficient increment is induced on certain regions of the fuselage and that pressure coefficients as high as 0.5 are developed on the jet surface of the type I terminal fairings.

It was stated previously that the type II and III terminal fairings were designed in a different manner from the type I. It was desired to obtain beneficial supersonic interference fields with the type II and III fairings and thereby reduce the drag at supersonic speeds. Comparison of the data in figures 11(a) and 11(b) indicates that this aim was accomplished. The increase in the level of the subsonic drag coefficient for the type III fairings, however, was undesirable and was probably

the result of separation of the boundary layer in the vicinity of the fairing inlet and inlet drag.

Performance at operating jet pressure ratios.- The data in figure 11 have all been presented for constant values of jet total-pressure ratio. Inasmuch as an airplane, when it is accelerating, would be operating at a different value of pressure ratio at each Mach number, the configurations are compared in figure 12 on this basis. The selected variation of jet total-pressure ratio with Mach number is presented in figure 12 for engine B of reference 8 at military power (nonafterburning).

The data indicate that the type I terminal fairings improve the drag coefficient of afterbody A by about 0.0030 at $M = 0.80$ (fig. 12(c)), show a loss of about 0.0015 near $M = 1.00$, and improve the drag coefficient again by about 0.0050 at a Mach number of 1.06. An airplane equipped with the type I terminal fairings should realize an improvement of about 13 percent in the subsonic cruise range at a Mach number of 0.90 over an airplane fitted with afterbody A. There should also be an increase in the supersonic performance, inasmuch as the drag coefficients for the type I terminal fairings are lower than those of configuration A. In addition, reference 7 indicates an improvement in performance for afterburner-on operation which would be required for operation at the supersonic speeds.

The type II fairings have about the same subsonic drag coefficient as afterbody B but show an improvement of about 0.0020 in drag coefficient at a Mach number of 1.06 (fig. 12(a)). It is surprising, but the type III fairings appear to be better than either the type II fairings or afterbody B at a Mach number of 1.06. Inspection of the pressure-coefficient data in figures 10(e) and 10(f) shows a strong expansion just inside the inlet of the scoop (rows 2 and 3) and a general recovery toward the base. The pressures measured on rows 2 and 3 appear to be much more negative when the fairings are in place than those for afterbody B with the fairings removed. A compensating effect may be that the pressures in the field outside the fairings are generally more positive than those for the basic body at the supersonic speeds, as evidenced by the data at rows 4, 5, and 7 (fig. 10(f)). These more positive pressures are probably also being experienced along the rearward portions of the horizontal and vertical tails, and thus cause a further improvement in the drag coefficient with the type III fairings installed.

For comparison, the drag coefficients for the type I fairing are plotted with afterbody B drag coefficients in figure 12(b), and it is noted that the type I fairings have a lower drag coefficient over most of the Mach number range investigated. Some of the possible reasons for this result have been noted previously.

Afterbody D was established in reference 6 as the best of the boattailed afterbodies, and this has been shown again herein. This afterbody is compared with the best of the terminal fairings (type I). (See fig. 12(d).) The data indicate that the type I terminal fairings are slightly better than afterbody D over most of the Mach number range investigated. The lower drag coefficients for the type I terminal fairings can be explained when it is noted that, as the jet pressure ratio increases, the drag coefficient for the type I terminal fairings decreases, whereas the drag coefficient of afterbody D generally increases substantially. (See fig. 8(a) and ref. 6.) It is reasoned that the jet-interference flow field is beneficial for the type I terminal fairings (see figs. 10(a) and 10(b)) but is detrimental to afterbody D (fig. 8(a)). This result (namely, that the type I terminal fairings have lower drag coefficients than the best boattailed afterbody (afterbody D)) is of practical significance, inasmuch as it indicates that a terminal-fairing installation can be constructed that is as good as or better than a good conventional afterbody. This could result in a good engine-terminal fairing combination being designed with fixed afterbody geometry, which might make a substantial saving in weight and complexity. The conclusion just stated has also been indicated in references 7 and 10. The performance improvement obtained with the use of afterbody terminal fairings indicates a need for further research on this type of afterbody-engine combination.

CONCLUSIONS

An investigation of a single-engine fighter model with a hot-jet exhaust in the Langley 16-foot transonic tunnel over a Mach number range from 0.80 to 1.10 has led to the following conclusions:

1. The drag of these airplane afterbodies (without terminal fairings) generally follows the same trends as simple boattailed bodies of revolution; however, interference effects of aerodynamic surfaces and protuberances can be large.

2. The application of afterbody terminal fairings to a highly boattailed conventional afterbody resulted in a reduction in drag coefficient over most of the Mach number range.

3. A comparison of the best of the terminal fairings with the best conventional boattailed afterbody indicated that the terminal fairing model had lower drag coefficients over most of the Mach number range.

4. The reduction in drag coefficient with the type I terminal fairings was the result of beneficial jet interference on the terminal bodies and on the fuselage ahead of the base.

Langley Research Center,
National Aeronautics and Space Administration,
Langley Field, Va., August 19, 1958.

[redacted]

APPENDIX

DESIGN CONCEPT OF TERMINAL FAIRINGS

Research results obtained in recent years indicate that most fuselages and nacelles for afterburning jet engines experience very important excessive base and boattail drags in afterburner-off cruising flight. As illustrated in sketch 1, the variable area primary nozzle is contracted in the nonafterburning operating condition to maintain the proper mass flow through the engine. This contraction of the exit area produces a

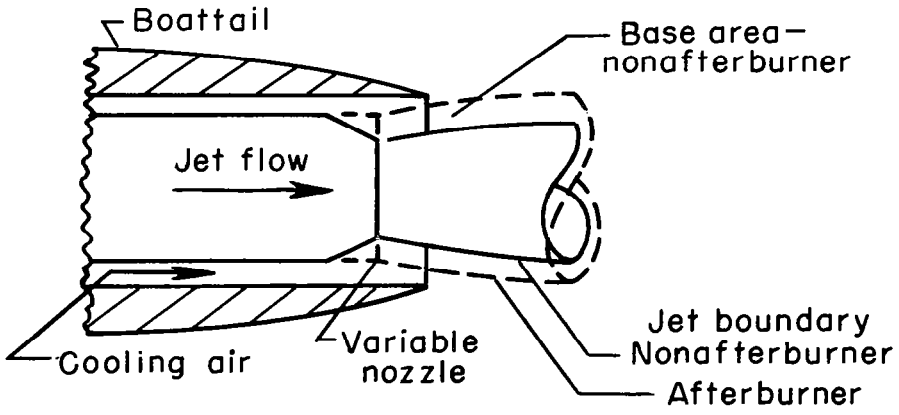

Sketch 1

large base area through which only a small amount of cooling air flow passes. For this type of configuration, the jet aspirates the flow over the base and in any separated region of the boattail to much lower pressures than would exist without the jet.

The terminal fairing idea is based on a combination of the transonic area rule and transonic wind-tunnel theories. As illustrated in sketch 2, several three-dimensional bodies, terminal fairings, "horns," or slotted afterbodies, as they are variously called, are extended rearward from the steep portion of the boattail to form a slotted surface surrounding the nozzle of the primary jet. According to the area rule theory, this addition to the body will effectively increase its fineness ratio and greatly reduce the effective slope of the boattail, reduce its pressure drag, and tend to eliminate flow separation. In addition,

[redacted]

the increase in pressure over the boattail, together with the elimination of flow separation, should cause a major increase in the pressures

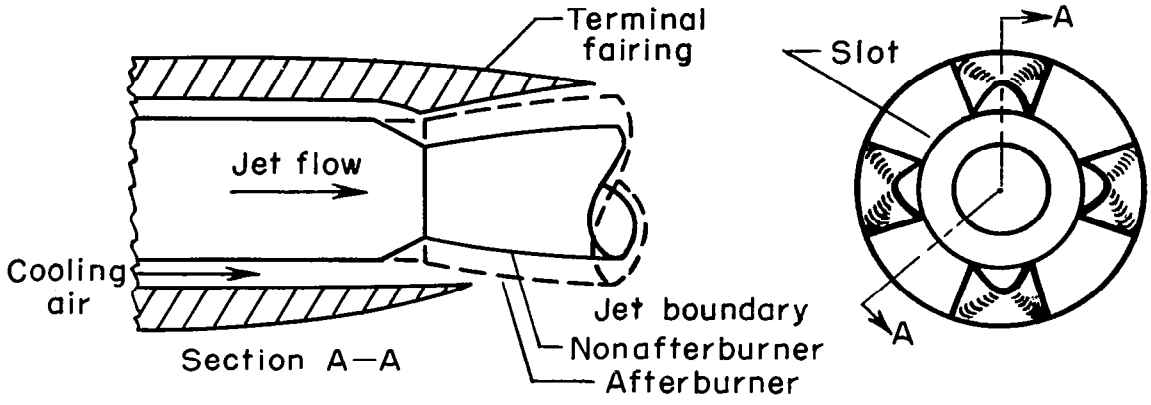

Sketch 2

over the base, reduce base drag, and also cause the jet effects to become favorable instead of unfavorable.

The terminal-fairing idea resembles the NACA transonic-wind-tunnel scheme in that the internal and external flows are not isolated rearward of the start of the slots. The external flow can penetrate the slotted surface to raise pressures over the rear portions of the boattail and the base. The jet flow also is not confined; therefore, separation losses due to overexpansion of the jet (such as occur in the case of the convergent-divergent nozzle below design pressure ratio) can be avoided. In addition, in afterburner operation at high jet pressure ratios (such as occur in supersonic flight), the high pressure flow at the exit nozzle will impinge on the rearward facing surfaces of the terminal fairings and produce thrust forces through the mechanism of increased surface pressures. Boundary-layer—shock-interaction effects can also produce thrust forces on the boattail regions. Thus, the fixed-geometry terminal fairings can provide a part of the thrust benefits of the diverging part of a convergent-divergent nozzle. The amount of thrust that can be recovered with such an arrangement is presently unknown.

In an attempt to apply these principles to an actual model and to avoid, if possible, the local acceleration of the flow experienced with

a preliminary design, the area distribution of the single-engine fighter model was utilized as indicated in the following sketch:

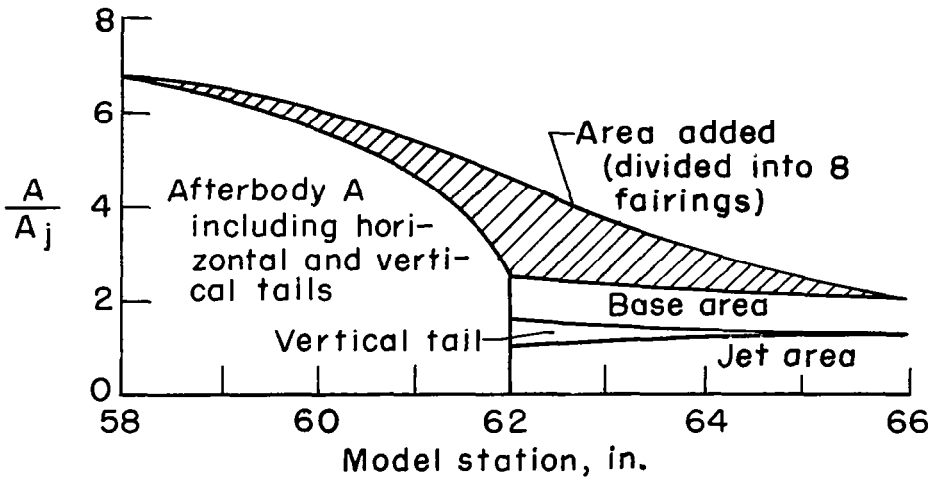

Sketch 3

The area distribution of the basic model has steep slopes and a large base annulus which is conducive to high afterbody drag. It was decided to add area between a certain body station where the slope was relatively low and the rearmost point of the vertical tail. The selection of both the start and ending of the area to be added was arbitrary, but some attention was given to limiting the length of the terminal fairings to something practical. The area added was to approximate the area of a Sears-Haack body (3/4-power series) between these two arbitrary points and was divided between eight terminal fairings. Because the angle of boattailing was not symmetrical about the jet axis (see figs. 3 and 4), the eight terminal fairings were not exactly similar. The lines of each were faired smoothly into the forward fuselage and an attempt was made to eliminate any increase in area on the streamwise surfaces. The coordinates of each terminal fairing are given in table I and a typical cross section of the fairings is given in figure 5. Reference 7 shows some performance data for more recent designs of this terminal-fairing idea utilizing both nonafterburning and afterburning primary nozzles and also discusses the refinements to these design concepts.

REFERENCES

1. Hearth, Donald P., and Gorton, Gerald C.: Investigation of Thrust and Drag Characteristics of a Plug-Type Exhaust Nozzle. NACA RM E53L16, 1954.

2. Salmi, Reino J.: Experimental Investigation of Drag of Afterbodies With Exiting Jet at High Subsonic Mach Numbers. NACA RM E54I13, 1954.

3. Henry, Beverly Z., Jr., and Cahn, Maurice S.: Preliminary Results of an Investigation at Transonic Speeds To Determine the Effects of a Heated Propulsive Jet on the Drag Characteristics of a Related Series of Afterbodies. NACA RM L55A24a, 1955.

4. Cubbage, James M., Jr.: Jet Effects on the Drag of Conical Afterbodies for Mach Numbers of 0.6 to 1.28. NACA RM L57B21, 1957.

5. Baughman, L. Eugene, and Kochendorfer, Fred D.: Jet Effects on Base Pressures of Conical Afterbodies at Mach 1.91 and 3.12. NACA RM E57E06, 1957.

6. Norton, Harry T., Jr., and Swihart, John M.: Effect of a Hot-Jet Exhaust on Pressure Distributions and External Drag of Several Afterbodies on a Single-Engine Airplane Model at Transonic Speeds. NACA RM L57J04, 1958.

7. Runckel, Jack F.: Preliminary Transonic Performance Results For Solid and Slotted Turbojet Nacelle Afterbodies Incorporating Fixed Divergent Jet Nozzles Designed for Supersonic Operation. NASA MEMO 10-24-58L, 1958.

8. Runckel, Jack F., and Swihart, John M.: A Hydrogen Peroxide Turbojet-Engine Simulator for Wind-Tunnel Powered-Model Investigations. NACA RM L57H15, 1957.

9. Swihart, John M.: Effect of Target-Type Thrust Reverser on Transonic Aerodynamic Characteristics of a Single-Engine Fighter Model. NACA RM L57J16, 1957.

10. Swihart, John M., and Nelson, William J.: Performance of Multiple Jet-Exit Installations. NACA RM L58E01, 1958.

TABLE I.- DEVELOPMENT OF TYPE I TERMINAL FAIRINGS

Fairing	Fairing station, in.	W, in.	Z, in.	R, in.	T, in.	θ, deg
1	0.698	0.36	0.08	3.00	2.92	12.00
	1.413	.68	.16	3.00	2.84	13.00
	2.031	.76	.24	3.00	2.76	14.50
	2.685	.89	.36	3.00	2.64	17.00
	3.365	1.04	.53	3.00	2.47	20.00
	4.029	1.55	1.02	3.00	1.98	30.00
	4.698	1.49	.87	2.98	2.11	29.00
	5.371	1.40	.72	2.94	2.22	27.50
	6.031	1.25	.55	2.88	2.33	25.00
	6.643	1.03	.39	2.80	2.41	21.21
	7.365	.61	.18	2.66	2.48	13.13
2 and 8	0	0	0	----	----	0
	.698	1.08	.06	2.94	2.88	21.17
	1.413	1.36	.10	2.92	2.82	27.00
	2.031	1.56	.14	2.90	2.76	31.24
	2.685	1.65	.24	2.90	2.66	32.98
	3.365	1.79	.40	2.90	2.50	36.10
	4.029	2.06	.92	2.90	1.98	41.58
	4.698	1.97	.77	2.88	2.11	39.93
	5.371	1.77	.64	2.86	2.22	36.00
	6.031	1.48	.50	2.83	2.33	30.22
	6.643	1.06	.38	2.79	2.41	21.80
	7.365	.52	.21	2.69	2.48	11.19
	7.909	0	0	2.54	2.52	0
3 and 7	0.698	0.93	0.07	3.11	3.04	17.17
	1.413	1.02	.13	3.08	2.95	19.02
	2.031	1.12	.20	3.06	2.86	20.91
	2.685	1.26	.29	3.04	2.75	24.00
	3.365	1.48	.49	3.04	2.55	28.35
	4.029	1.82	1.04	3.02	1.98	35.08
	4.698	1.77	.87	2.98	2.11	34.65
	5.371	1.60	.72	2.94	2.22	31.50
	6.031	1.31	.57	2.90	2.33	26.16
	6.643	.90	.45	2.86	2.41	18.17
	7.365	.46	.24	2.72	2.48	9.73
4 and 6	0.698	0.87	0.07	3.76	3.69	13.35
	1.413	.99	.14	3.64	3.50	15.88
	2.031	1.07	.22	3.56	3.34	17.34
	2.685	1.08	.39	3.49	3.10	17.91
	3.365	1.31	.63	3.42	2.79	22.00
	4.029	1.57	1.37	3.35	1.98	27.13
	4.698	1.48	1.16	3.27	2.11	26.16
	5.371	1.30	.95	3.17	2.22	23.75
	6.031	1.05	.73	3.06	2.33	19.82
	6.643	.78	.53	2.94	2.41	15.20
	7.365	.43	.26	2.74	2.48	8.95
5	0.698	0.63	0.08	3.62	3.54	10.00
	1.413	.79	.18	3.54	3.36	12.78
	2.031	.82	.32	3.50	3.18	13.50
	2.685	.89	.54	3.46	2.92	14.75
	3.365	1.13	.83	3.41	2.58	19.00
	4.029	1.56	1.38	3.36	1.98	26.88
	4.698	1.47	1.19	3.30	2.11	25.75
	5.371	1.23	1.00	3.22	2.22	22.00
	6.031	.98	.79	3.12	2.33	18.11
	6.643	.71	.59	3.00	2.41	13.50
	7.365	.37	.30	2.78	2.48	7.70

TABLE II.- PRESSURE-ORIFICE LOCATIONS ON AFTERBODIES

[d_j = 2.615 in.]

(a) Afterbody A and type I terminal fairings

Fairing 1						Fairing 7		Afterbody between fairings 7 and 8 at ϕ = 292°	
Jet surface		Stream surface		Surface at ϕ = 345°		Surface at ϕ = 295°			
l, in.	l/d_j	l, in.	l/d_j	l, in.	l/d_j	l, in.	l/d_j	l, in.	l/d_j
0.96	0.344	1.62	0.620	0.18	0.069	0.18	0.069	-0.18	-0.069
1.62	.620	2.32	.887	.90	.344	.90	.344	-.60	-.229
3.06	1.170	3.80	1.453	1.62	.620	3.80	1.453	-1.20	-.459
3.80	1.453			3.06	1.170			-2.31	-.883
								-4.05	-1.553
								-5.65	-2.165

(b) Afterbody B and type II terminal fairings

Row 2			Base tubes			Fairing 2									
						Jet surface		Stream surface		Surface at ϕ = 60°		Surface at ϕ = 90°		Base	
ϕ, deg	l, in.	l/d_j	ϕ, deg	l, in.	l/d_j	l, in.	l/d_j	l, in.	l/d_j	l, in.	l/d_j	l, in.	l/d_j	l, in.	l/d_j
61	-1.499	-0.573	42	0	0	-0.518	0.198	-1.95	-0.746	-1.95	-0.746	-1.95	-0.746	2.51	0.960
61	-.832	-.318				2.01	.769	-.02	-.008	-.02	-.008	-.02	-.008		
61	-.165	-.063						.518	.198	.518	.198	.518	.198		
								2.01	.769	2.01	.769	2.01	.769		

(c) Afterbody B and type III terminal fairings

Under fairings						Base tubes		
Row 2			Row 3					
ϕ, deg	l, in.	l/d_j	ϕ, deg	l, in.	l/d_j	ϕ, deg	l, in.	l/d_j
19	-2.165	-0.828	61	-2.165	-0.828	42	0	0
19	-1.499	-.573	61	-1.499	-.573	--	--	--
19	-.832	-.318	61	-.832	-.318	--	--	--
19	-.165	-.063	61	-.165	-.063	--	--	--

Between fairings								
Row 4			Row 5			Row 7		
ϕ, deg	l, in.	l/d_j	ϕ, deg	l, in.	l/d_j	ϕ, deg	l, in.	l/d_j
255	-5.66	-2.167	90	-2.165	-0.828			
255	-3.79	-1.453	90	-1.499	-.573	148	-1.499	-0.573
255	-2.47	-.943	90	-.832	-.318	148	-.832	-.318
255	-1.27	-.485	90	-.165	-.063	148	-.165	-.063
255	-.33	-.127	90					

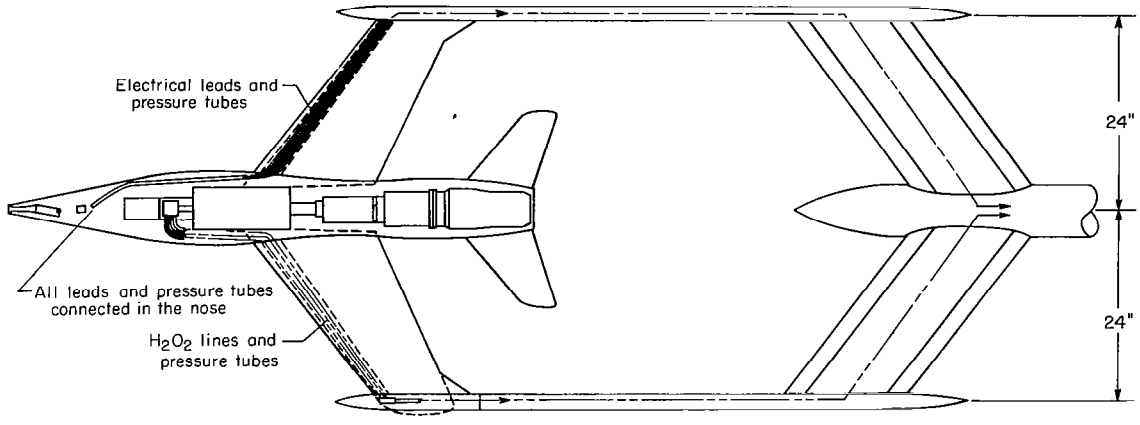

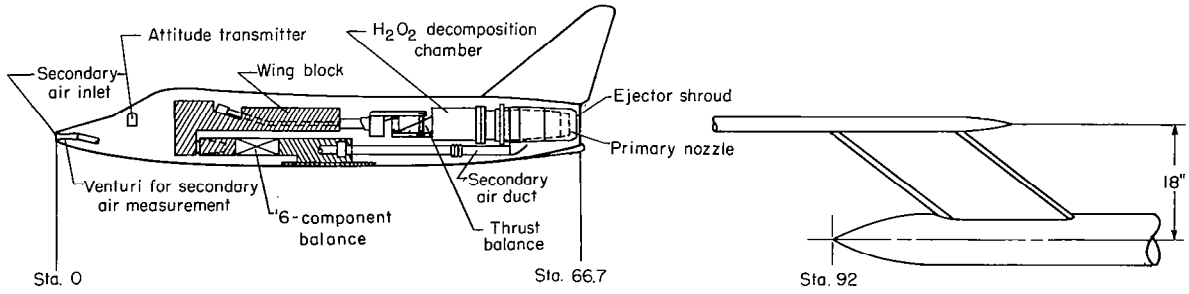

WING	
Wing area, (nominal), S	4.44 sq ft
AR	4.00
$\Lambda_{c/4}$	35°
c_r	17.273 in.
c_t	8.636 in.
NACA 65A006 airfoil sections - streamwise with 2.4 %c leading-edge camber	
Taper ratio	0.50
A_j/S (non-afterburning)	0.00839

FUSELAGE	
Length	66.7 in.
Max. height	9.0 in.
Max. width	8.6 in.
Area ruled for M = 1.0	

VERTICAL TAIL	
$\Lambda_{c/4}$	44°, 27"
Root section	NACA 0006
Tip section	NACA 0006
c_r	14.000 in.
c_t	2.480 in.
Taper ratio	0.18

HORIZONTAL TAIL	
$\Lambda_{c/4}$	35°
Root section	NACA 65A006
Tip section	NACA 65A004
c_r	9.893 in.
c_t	3.960 in.
AR	3.50
Taper ratio	0.40
i_t	-1.50°

Figure 1.- Sketch of jet-exhaust simulator model and support system.

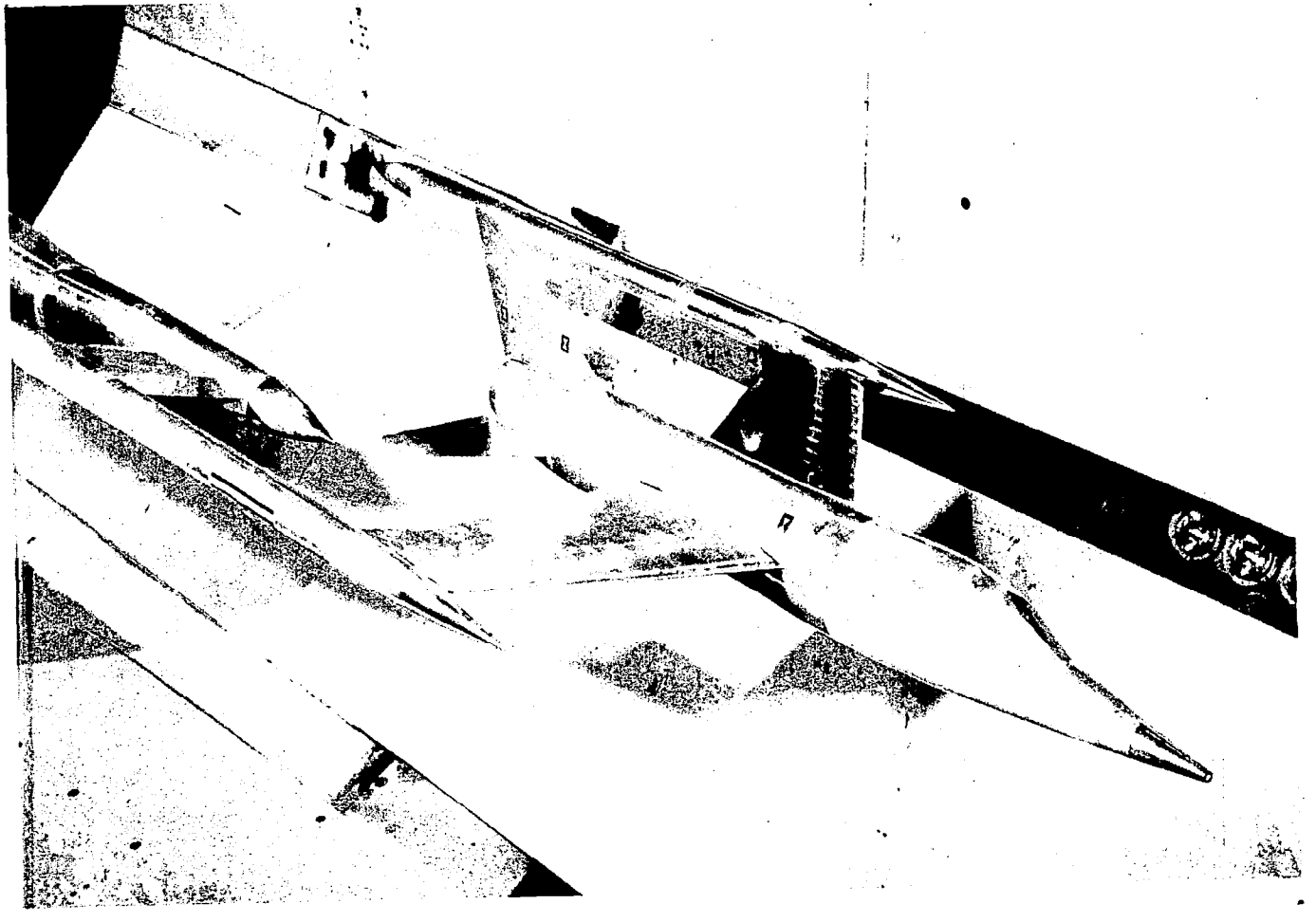

(a) Three-quarter front view with afterbody B. L-89404.1

Figure 2.- Photograph of single-engine fighter jet exhaust model mounted on bifurcate sting support in Langley 16-foot transonic tunnel.

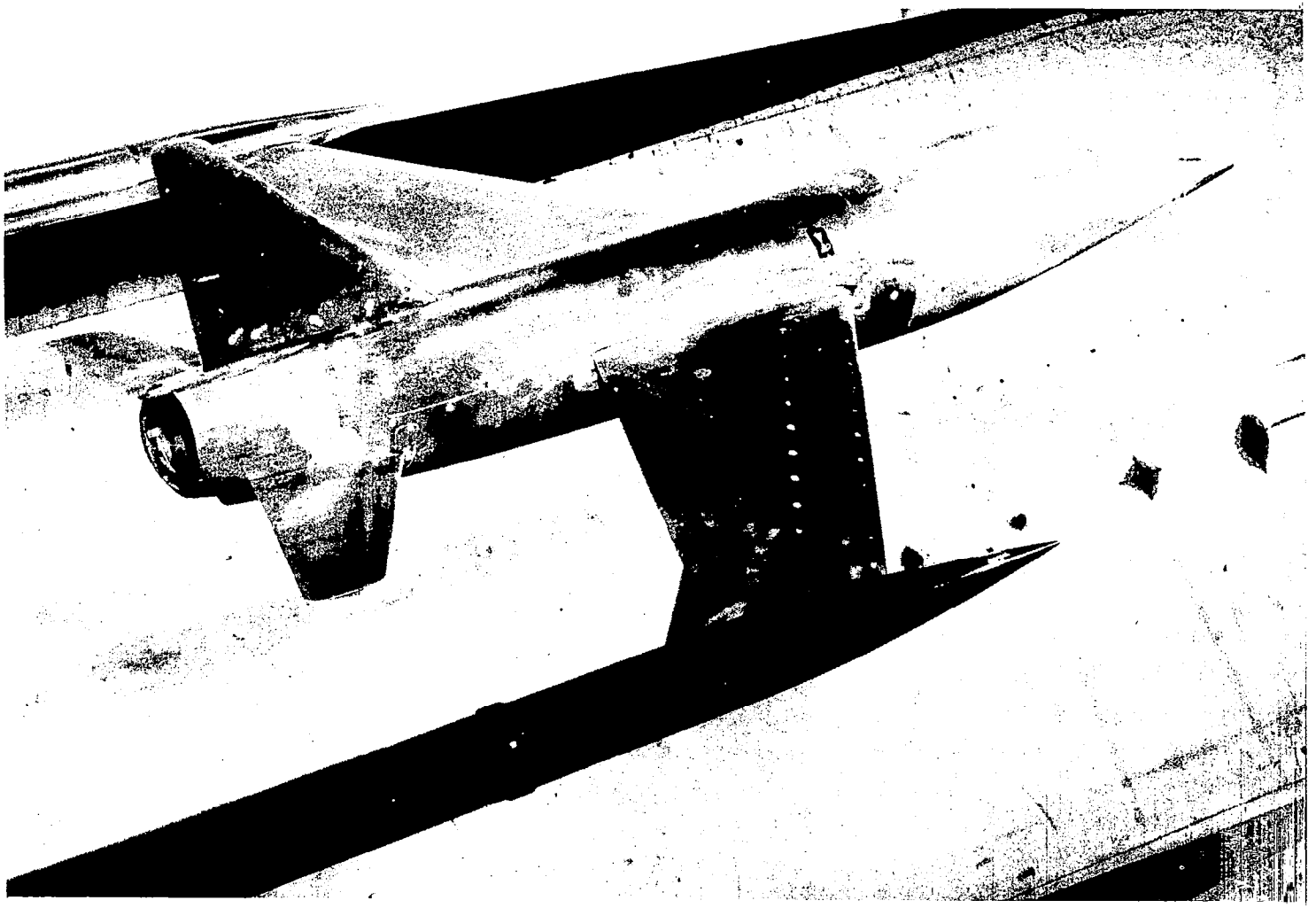

(b) Three-quarter rear view with afterbody D. L-92107

Figure 2.- Continued.

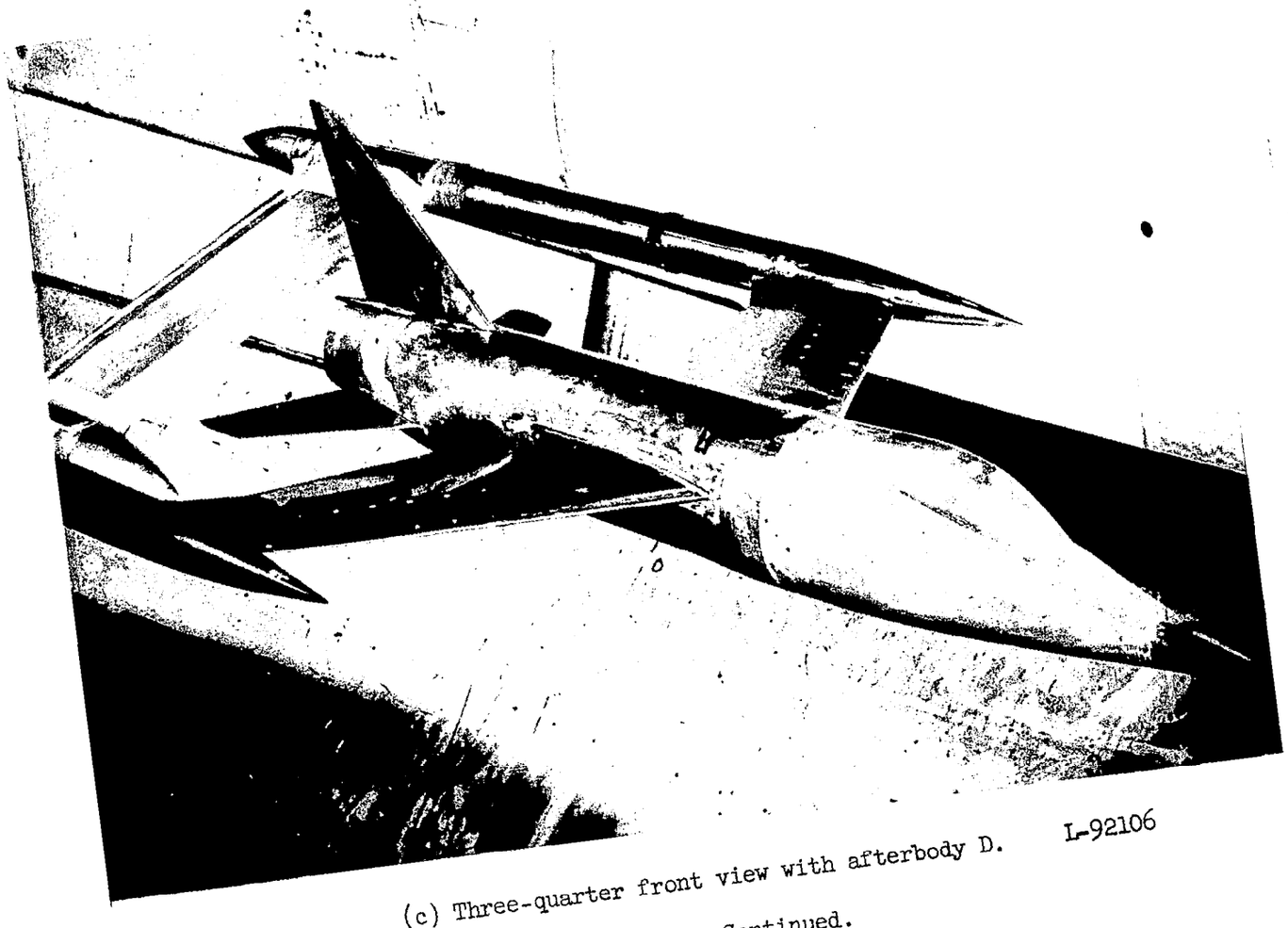

L-92106

(c) Three-quarter front view with afterbody D.

Figure 2.- Continued.

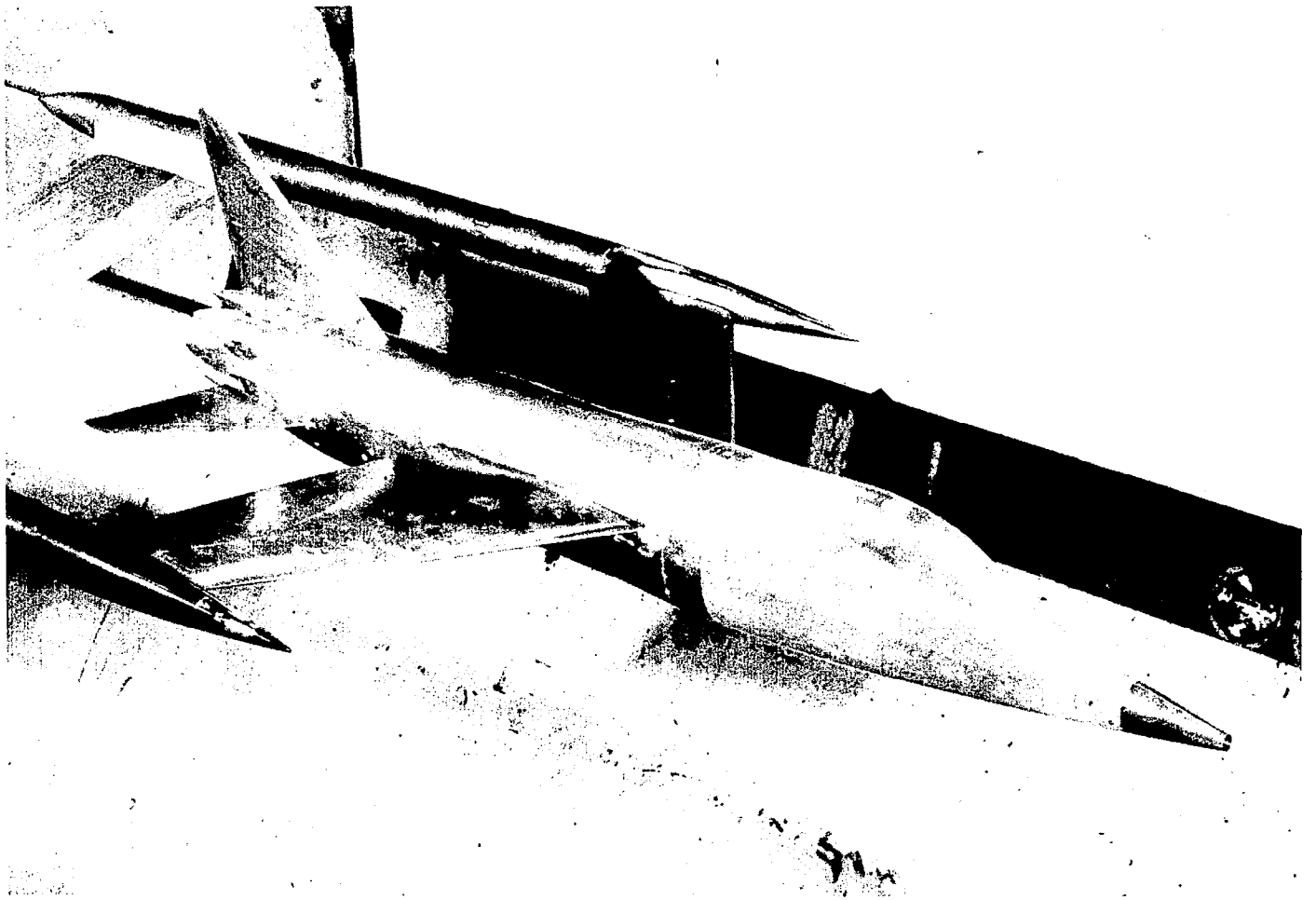

L-95252

(d) Three-quarter front view with afterbody A and type I terminal fairings.

Figure 2.- Continued.

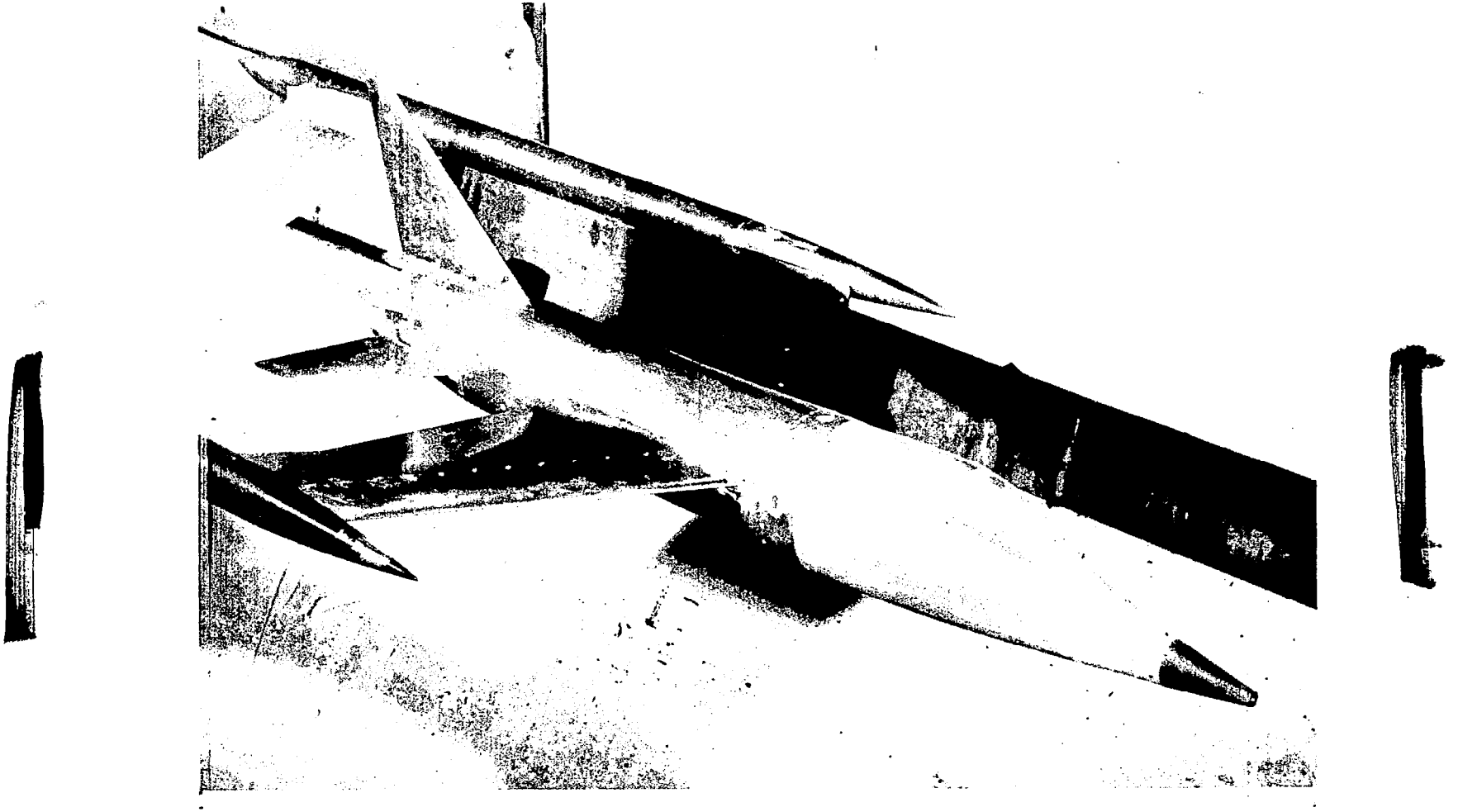

L-95249

(e) Three-quarter front view with afterbody B and type II terminal fairings.

Figure 2.- Continued.

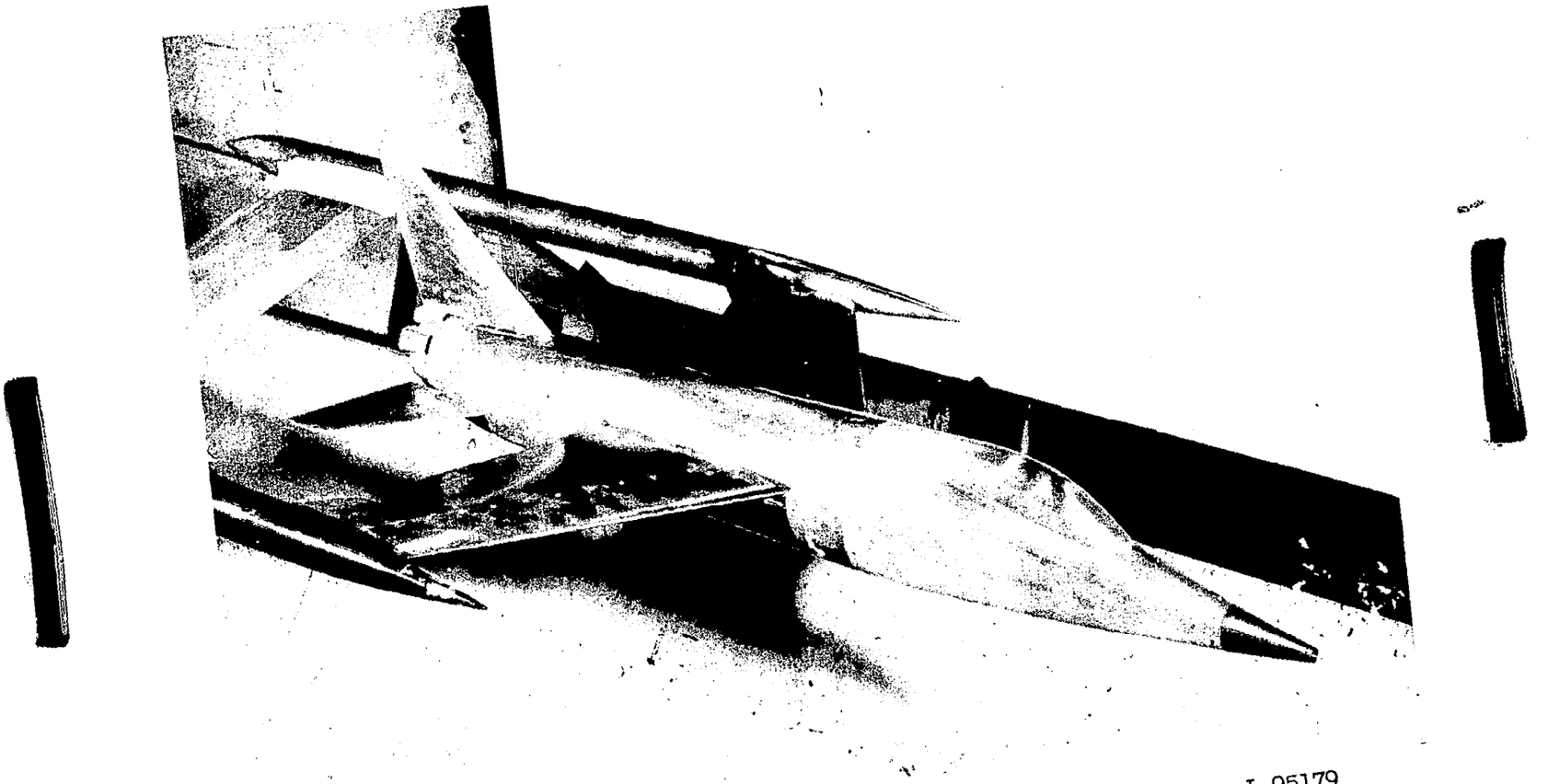

L-95179

(f) Three-quarter front view with afterbody B and type III terminal fairings.

Figure 2.- Concluded.

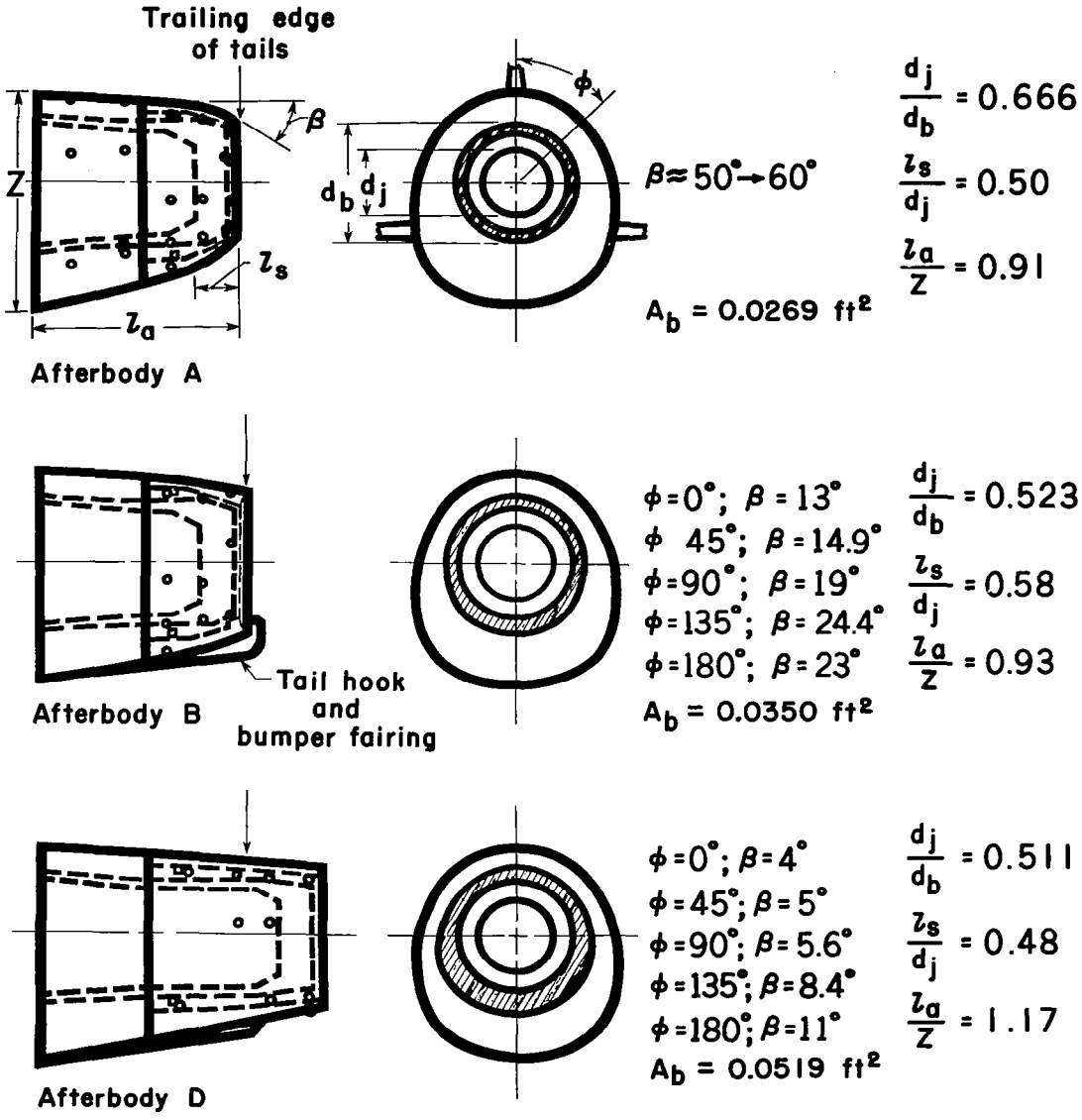

Figure 3.- Afterbody physical characteristics and dimensions.

Afterbody A

Afterbody B

Afterbody D

(a) Conventional afterbodies. L-58-2531

Figure 4.- Photographs of the three afterbodies and three types of terminal fairings.

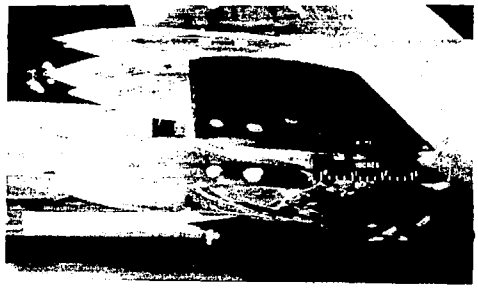

Type I

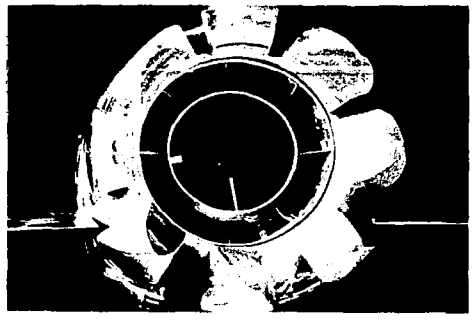

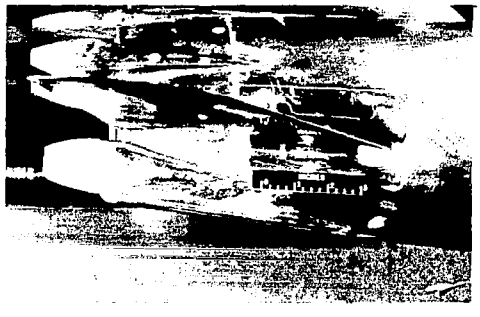

Type II

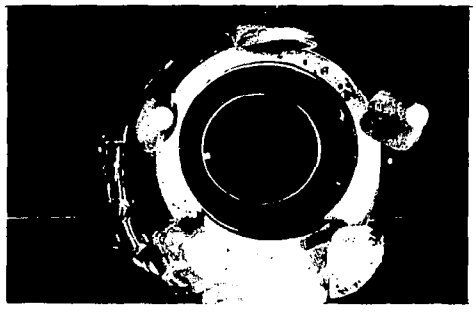

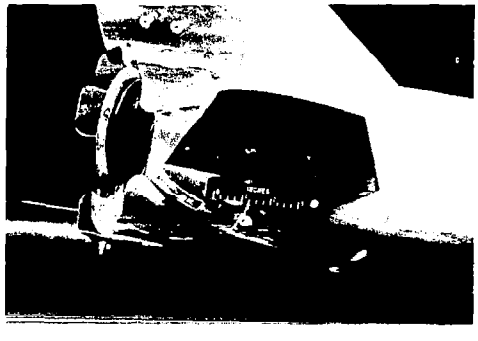

Type III

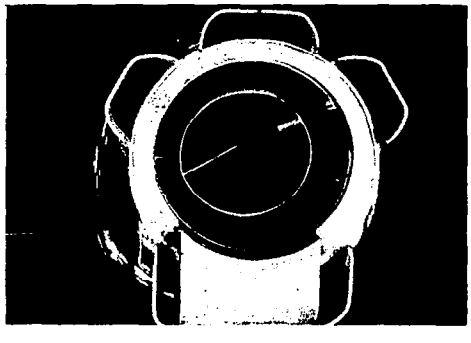

(b) Terminal fairings. L-58-2532

Figure 4.- Concluded.

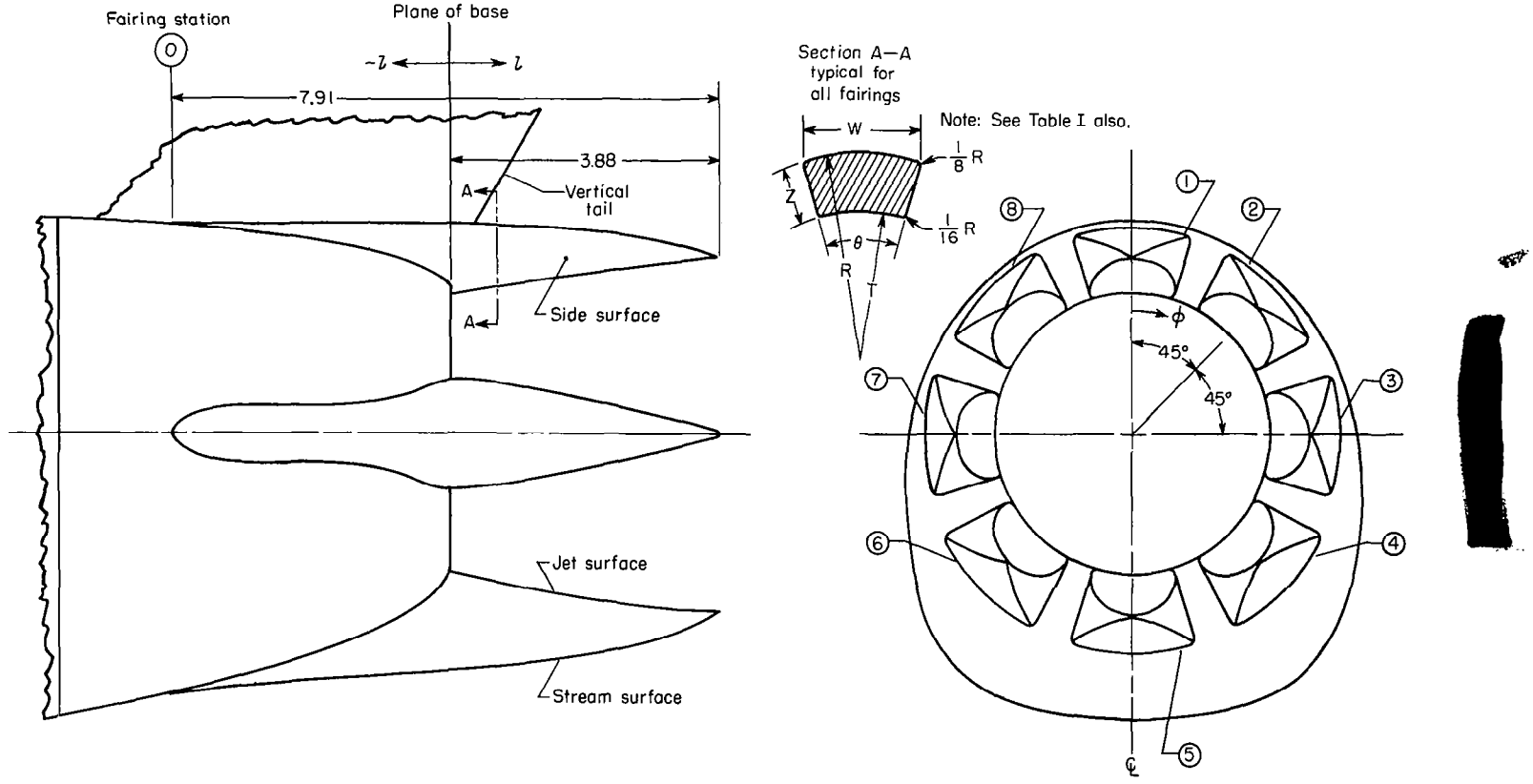

(a) Type I terminal fairings, dimensions, and typical cross section. See table I for dimensions and table II for orifice locations.

Figure 5.- Sketches of terminal fairings.

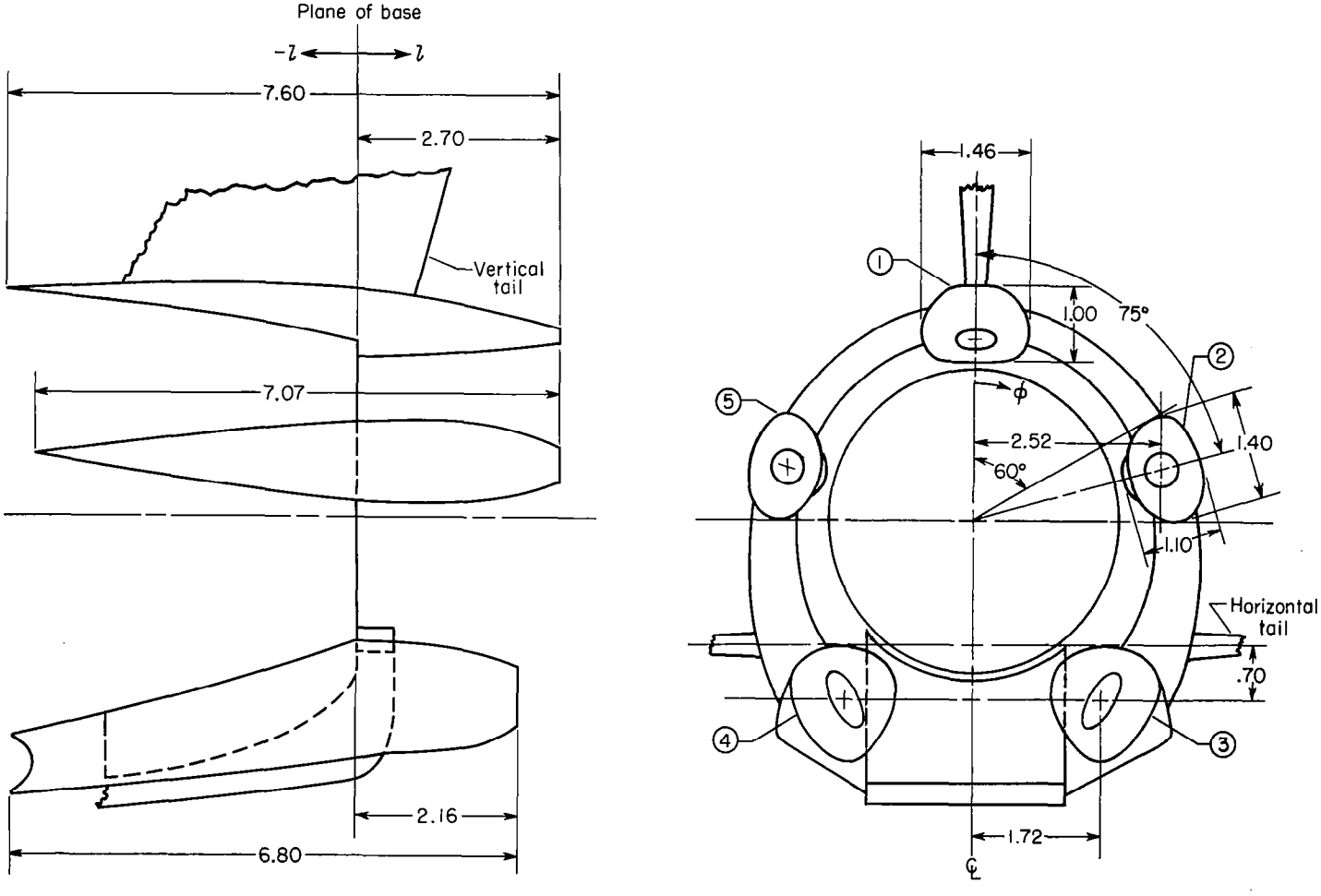

(b) Type II terminal fairings, dimensions, and general contour. See table II for orifice locations.

Figure 5.- Continued.

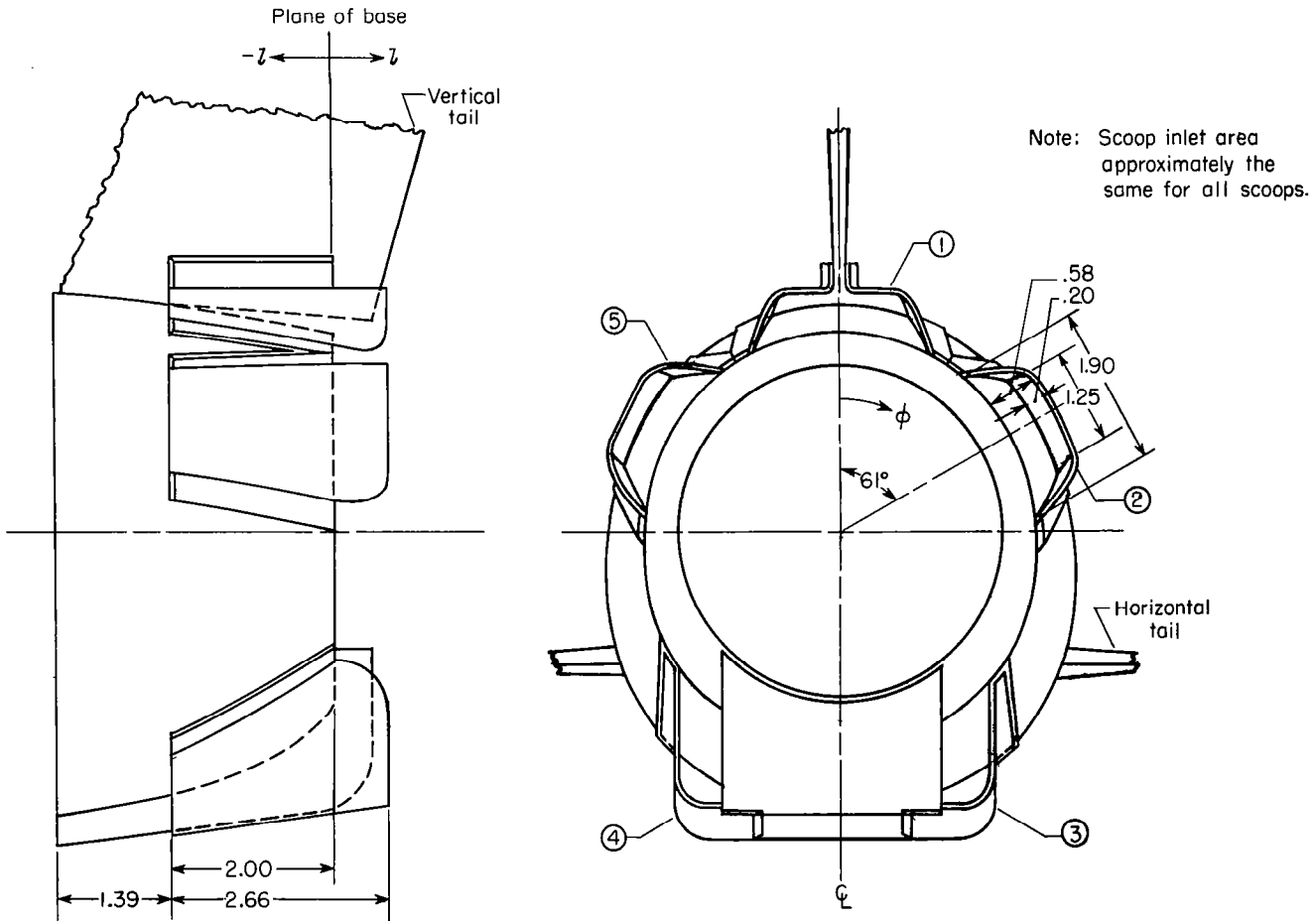

(c) Type III terminal fairings, dimensions, and general contours. Orifice locations are same as for afterbody B shown in table II.

Figure 5.- Concluded.

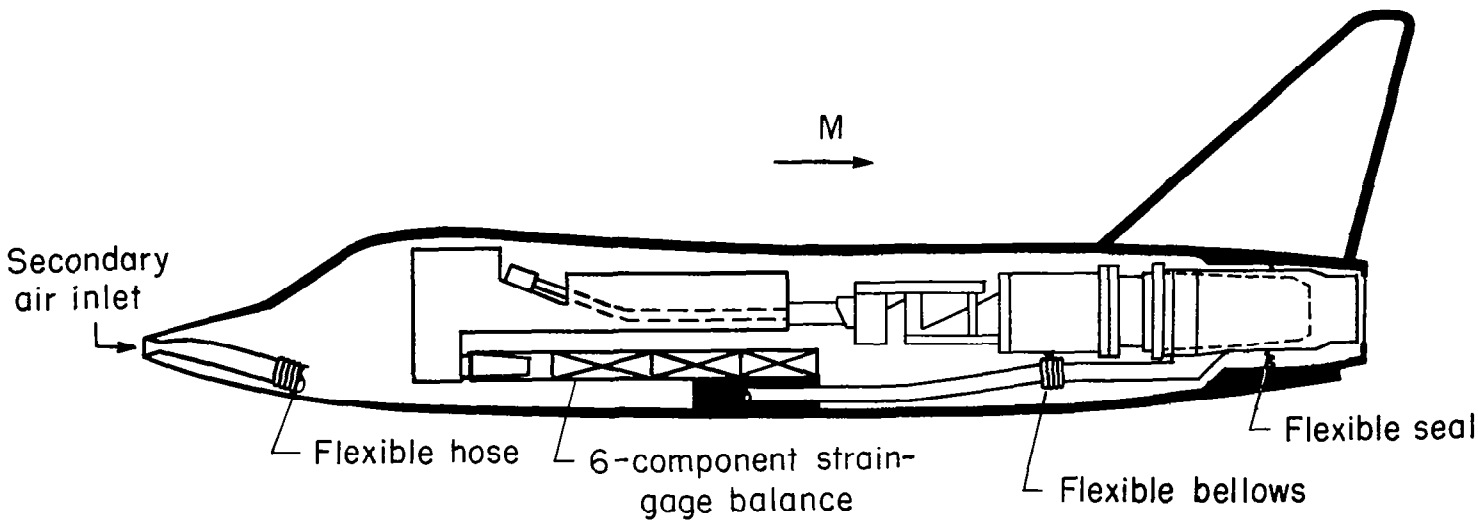

(a) External drag system.

Figure 6.- Schematic diagram of model showing locations of 6-component balance, pressures, and areas.

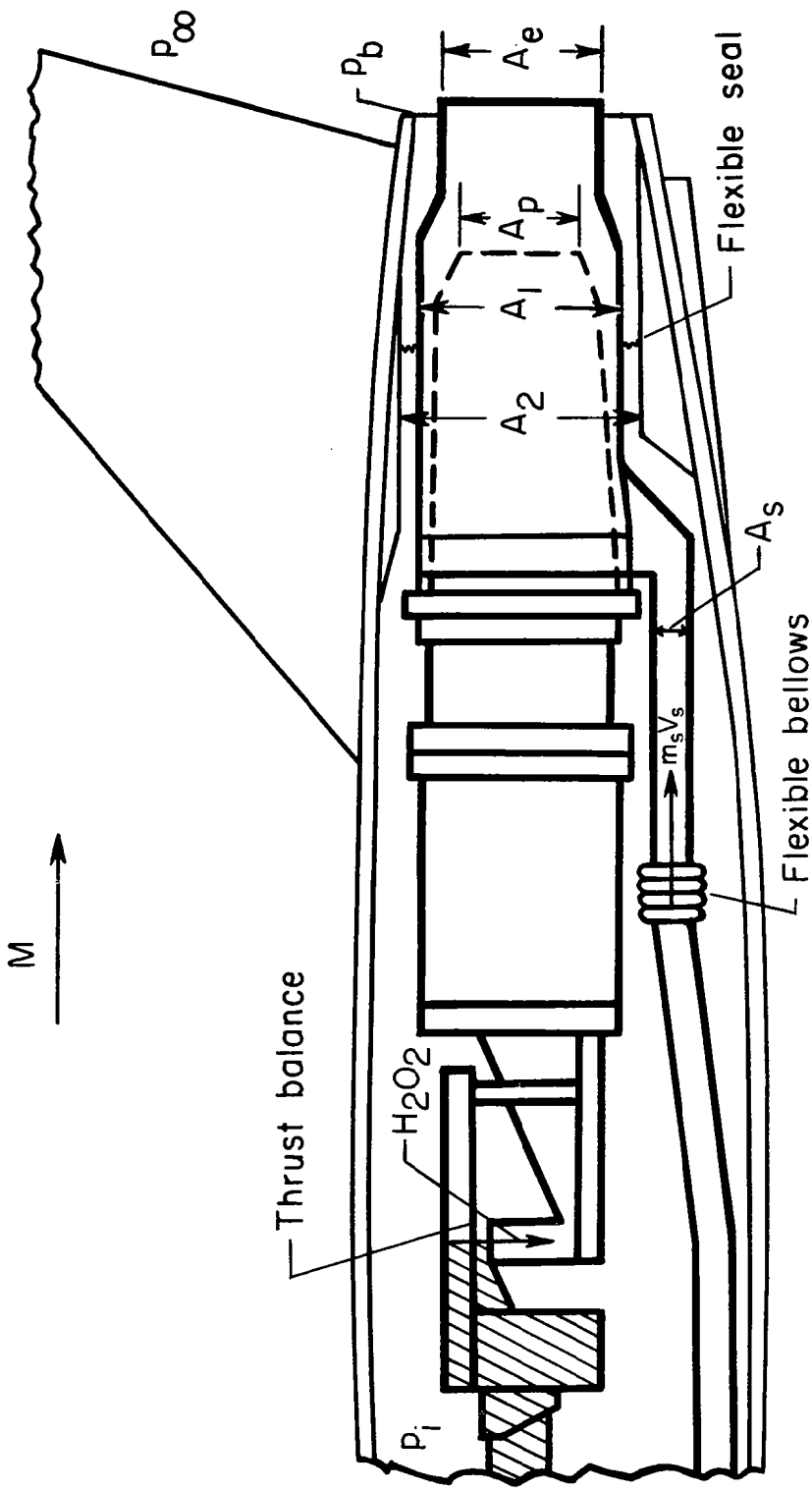

(b) Location of pressure measurements and areas.

Figure 6.- Concluded.

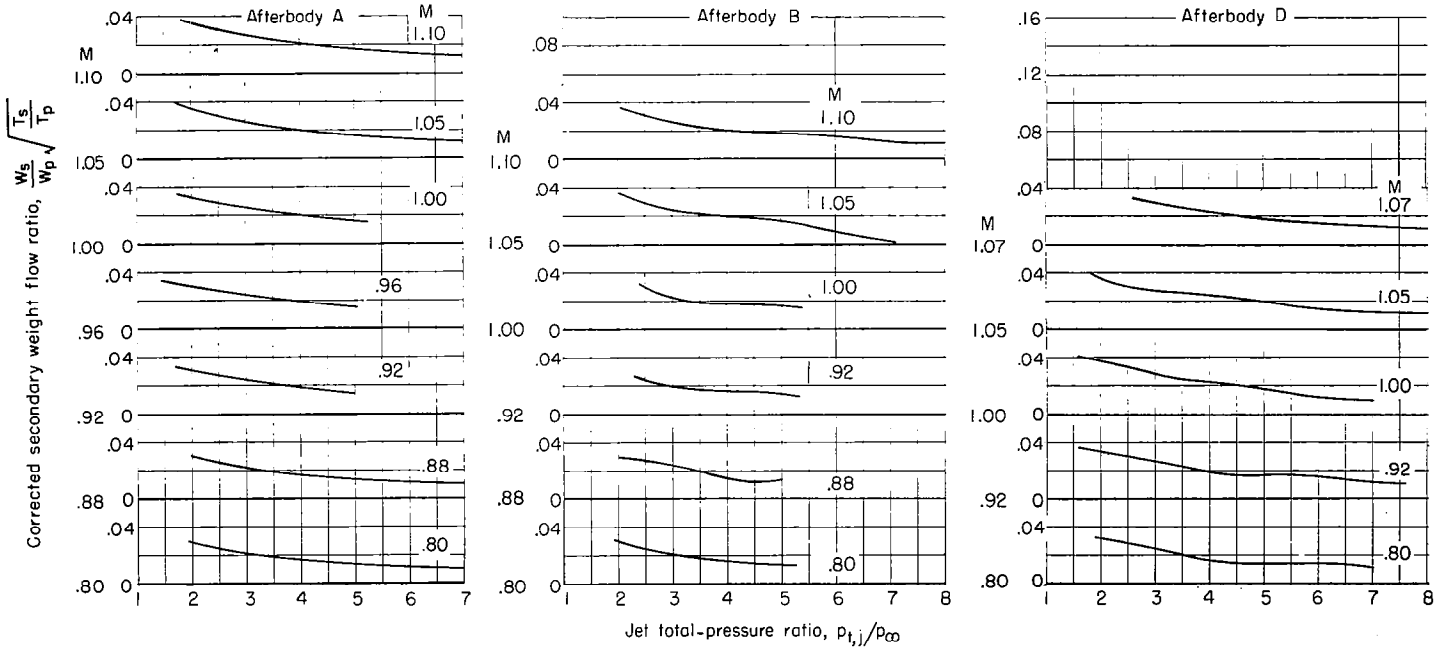

Figure 7.- Variation of the corrected secondary weight-flow ratio with primary total-pressure ratio for all afterbodies.

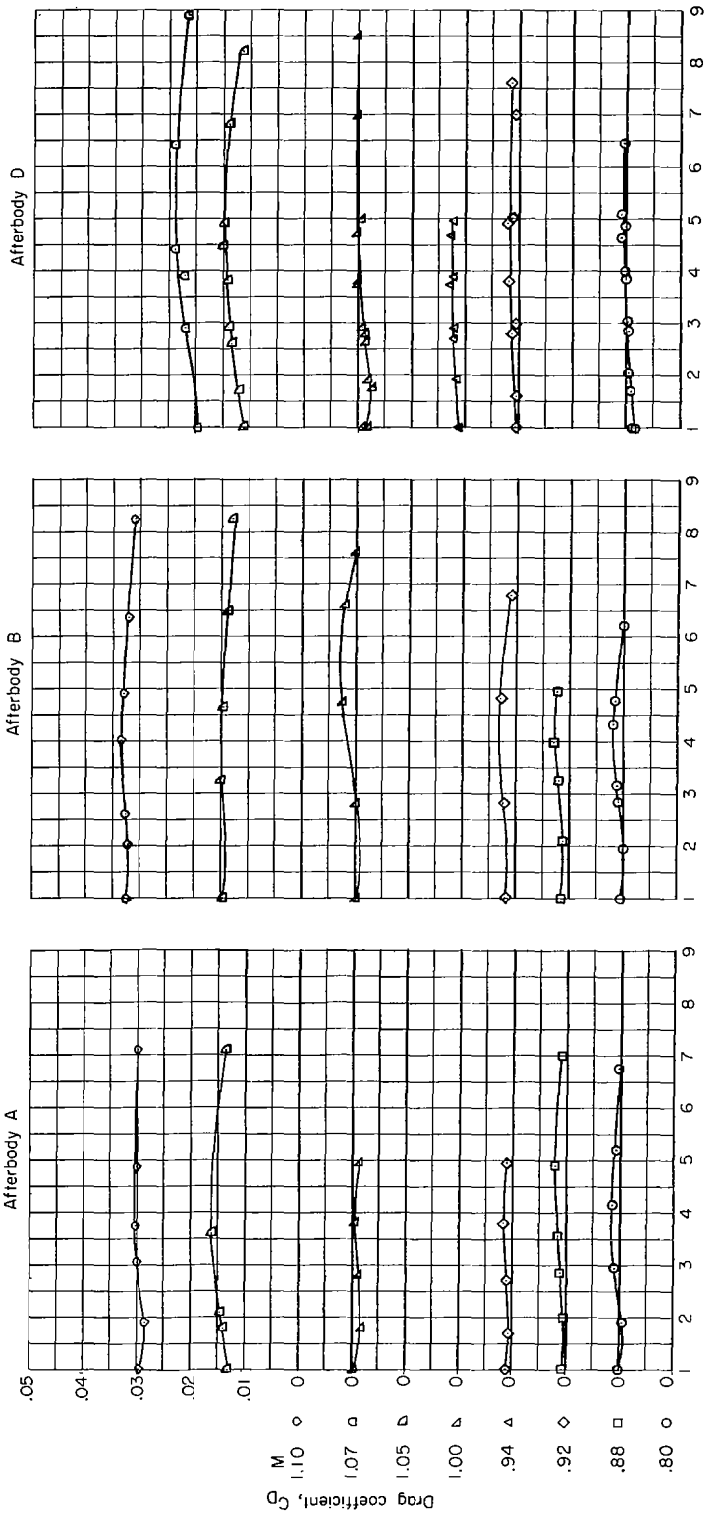

(a) Afterbodies A, B, and D.

Figure 8.- Effect of pressure ratio on drag coefficient for several afterbodies and Mach numbers.

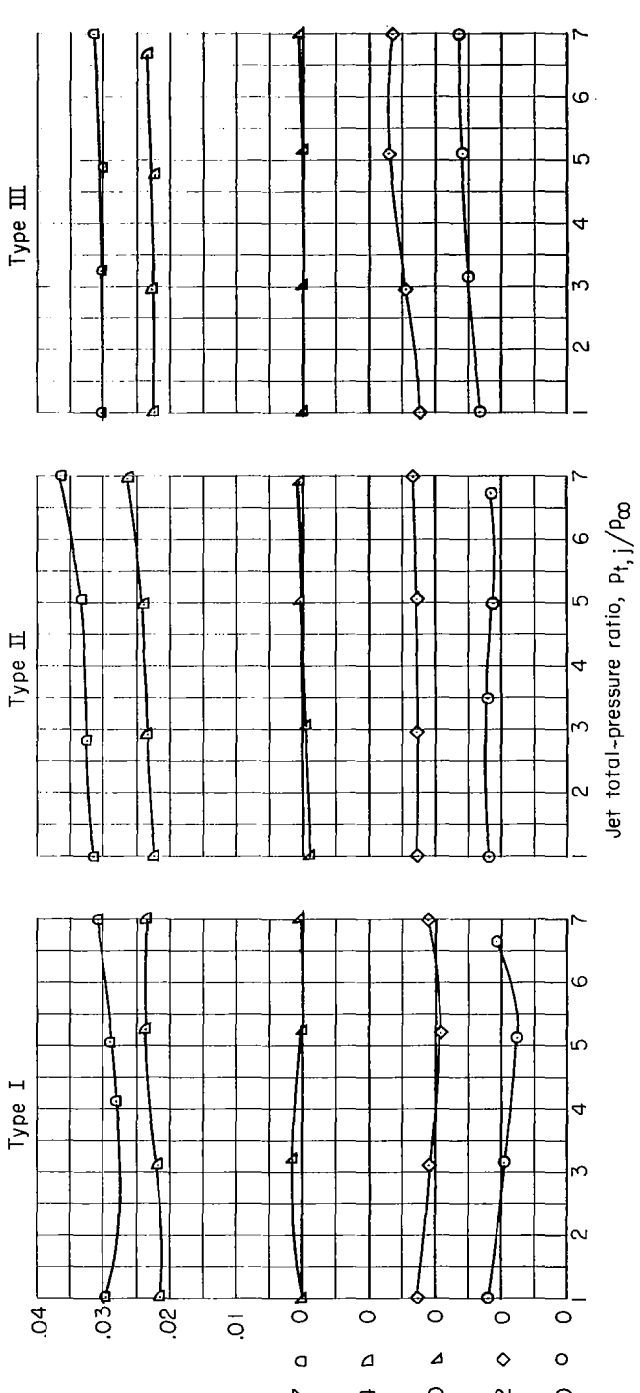

(b) Terminal fairings.

Figure 8.- Concluded.

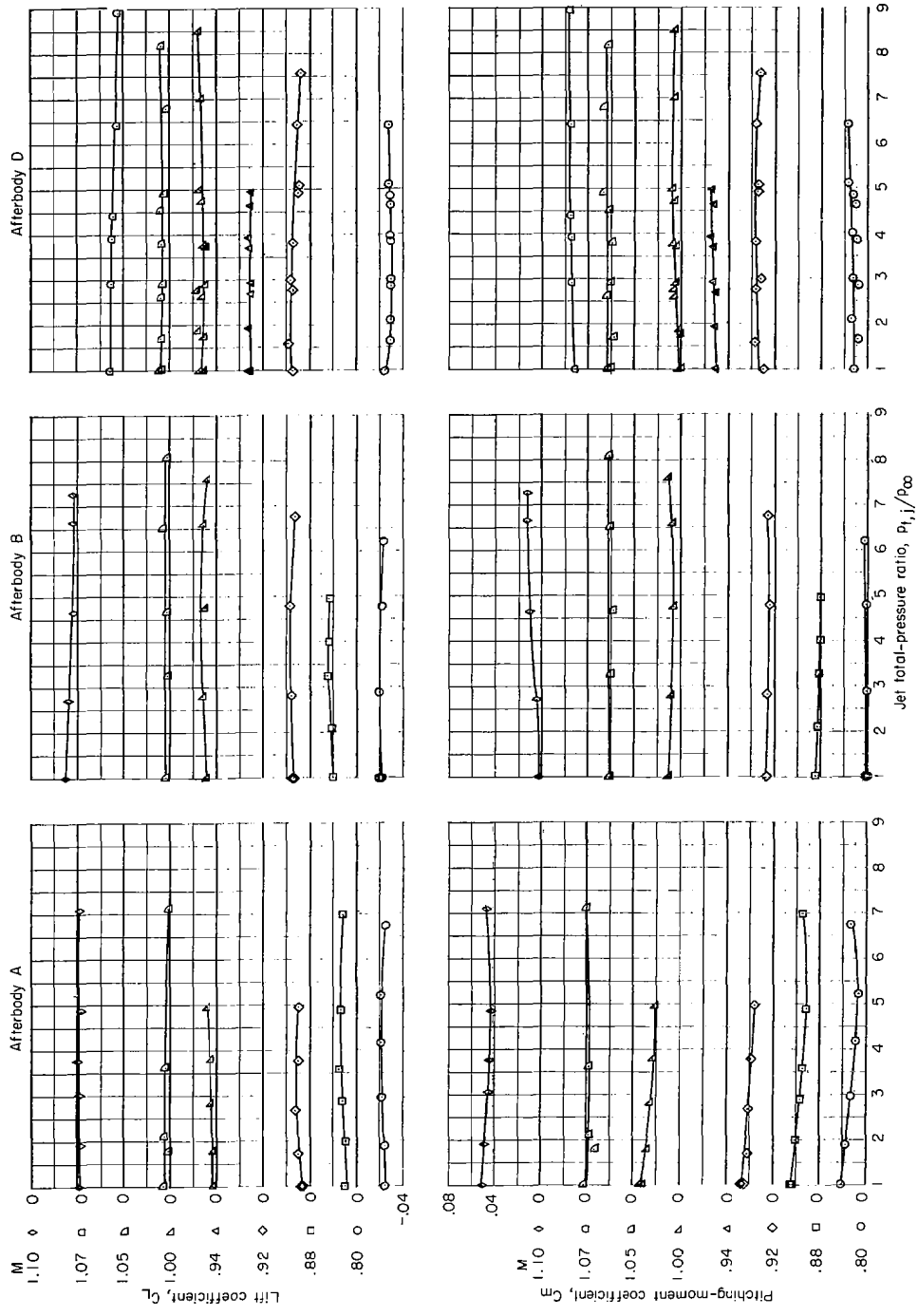

(a) Afterbodies A, B, and D.

Figure 9.- Effect of jet pressure ratio on pitching moment and lift coefficient for several afterbodies and Mach numbers.

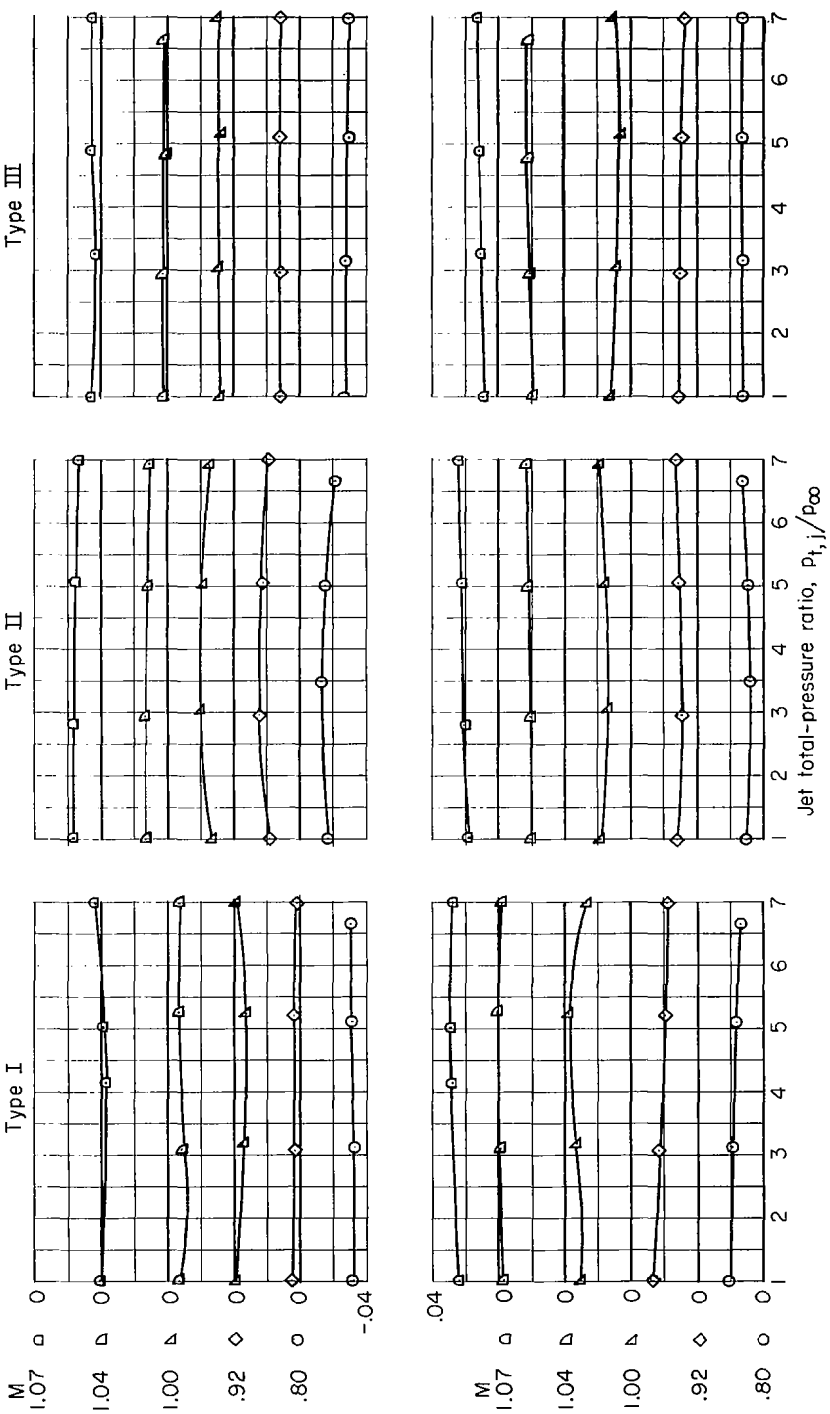

(b) Terminal fairings.

Figure 9.- Concluded.

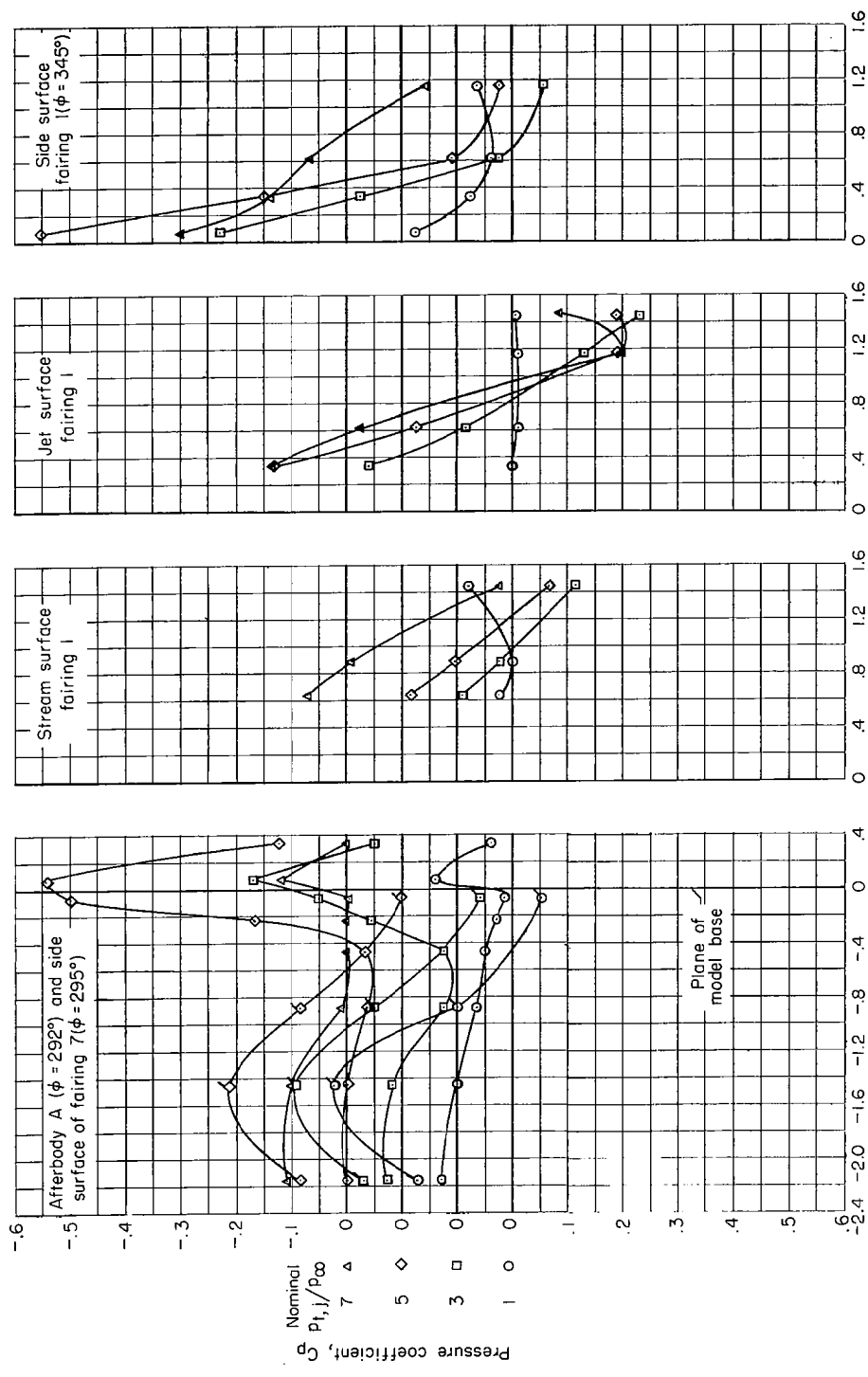

(a) M = 0.80; afterbody A and type I terminal fairings; flagged symbols, afterbody A alone.

Figure 10.- Variation of pressure coefficient over the afterbodies and terminal fairings at several values of jet total-pressure ratio.

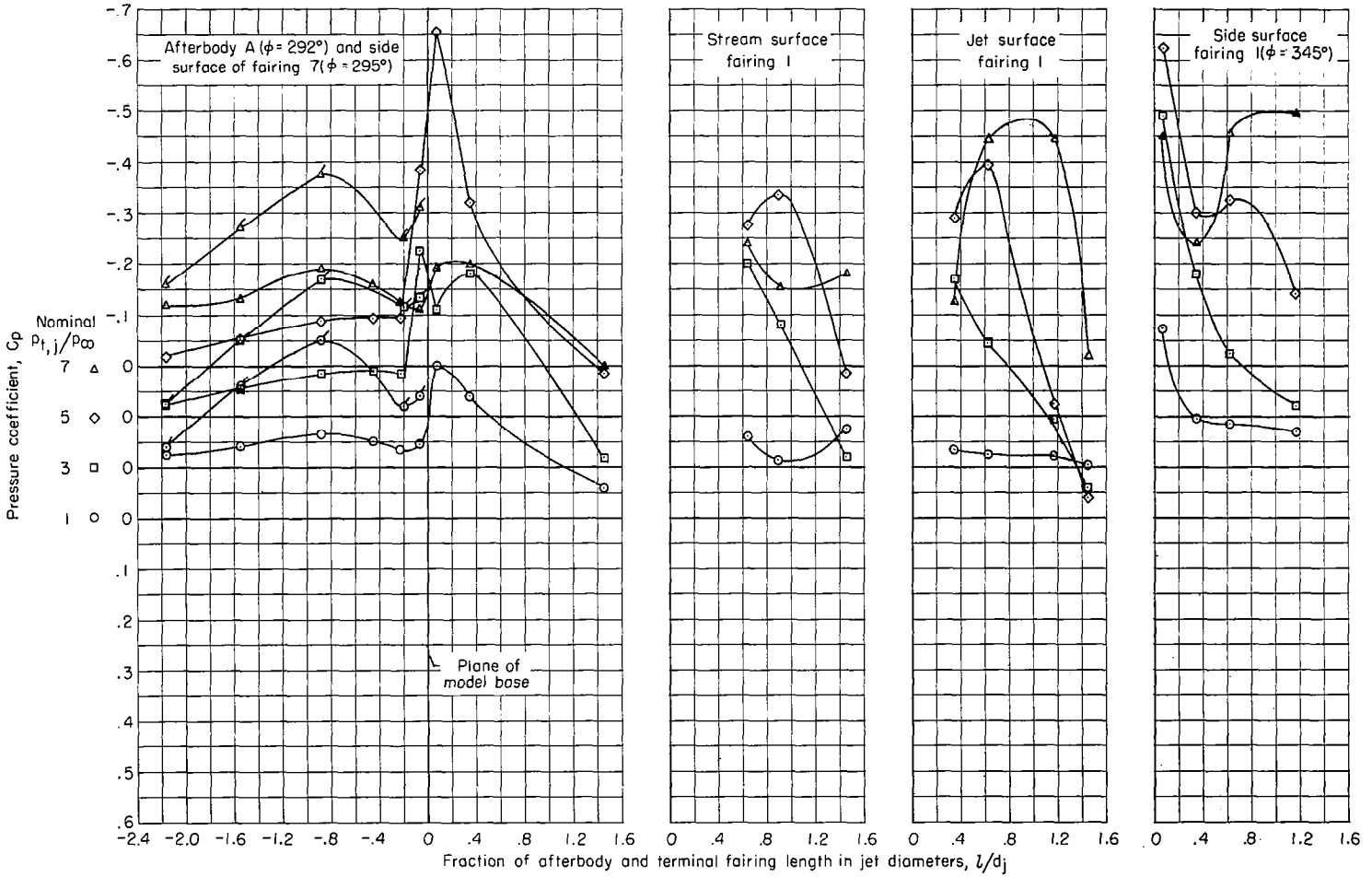

(b) M = 1.05; afterbody A and type I terminal fairings; flagged symbols, afterbody A alone.

Figure 10.- Continued.

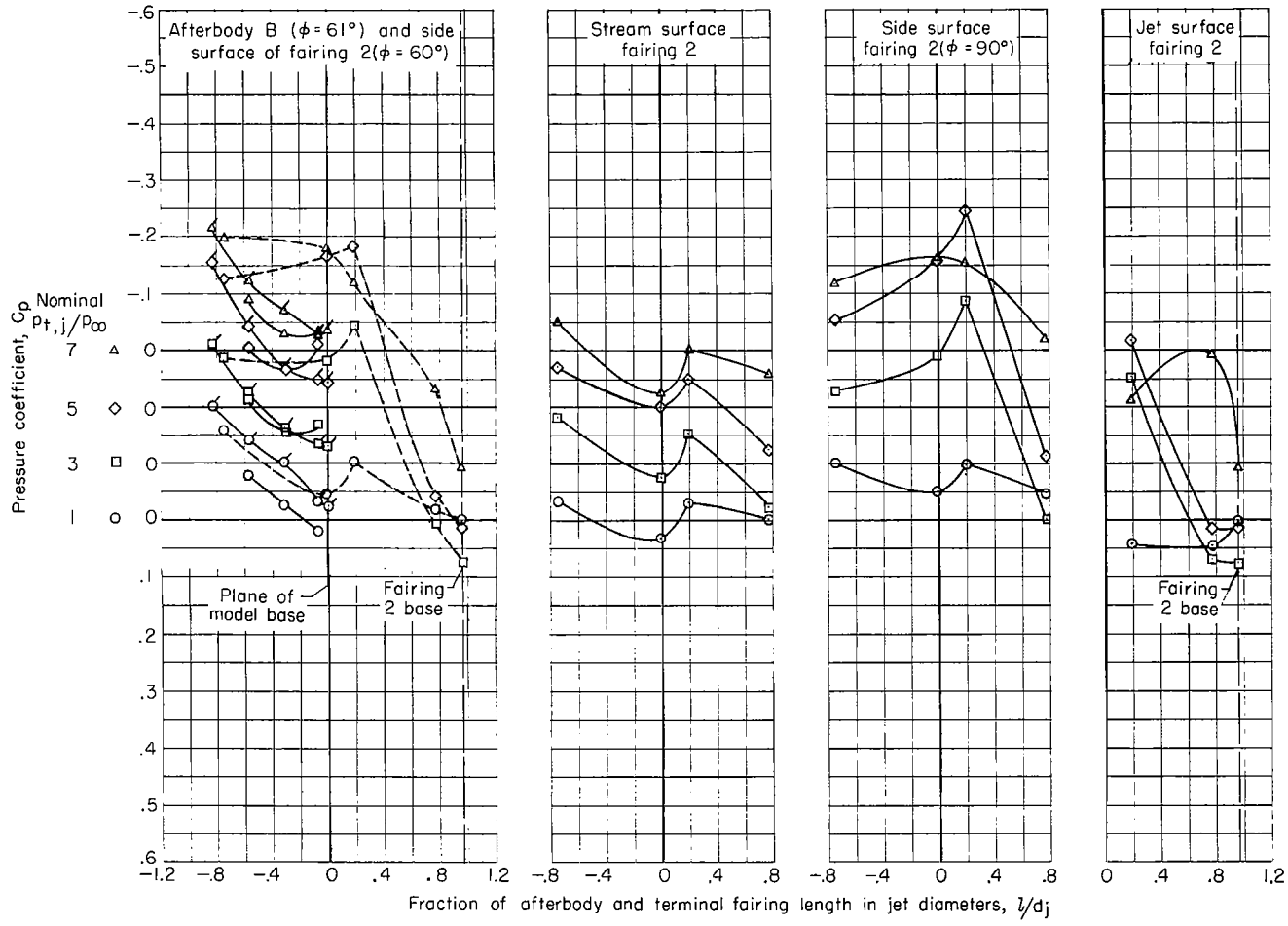

(c) M = 0.80; afterbody B and type II terminal fairings; flagged symbols, afterbody B alone; dashed line is fairing 2 surface (ϕ = 60°).

Figure 10.- Continued.

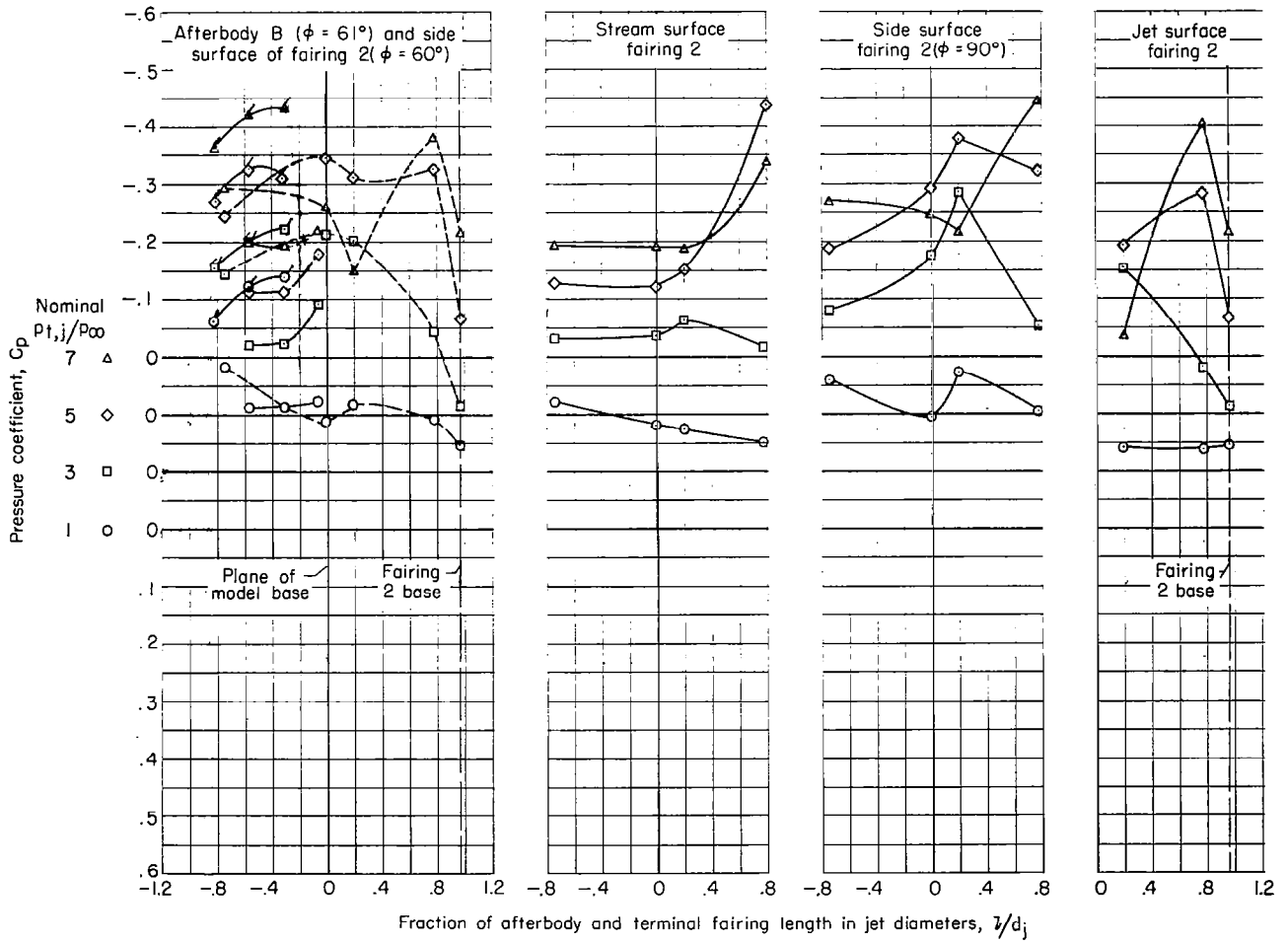

(d) M = 1.04; afterbody B and type II terminal fairings; flagged symbols, afterbody B alone; dashed line is fairing 2 surface ($\phi = 60^{\circ}$).

Figure 10.- Continued.

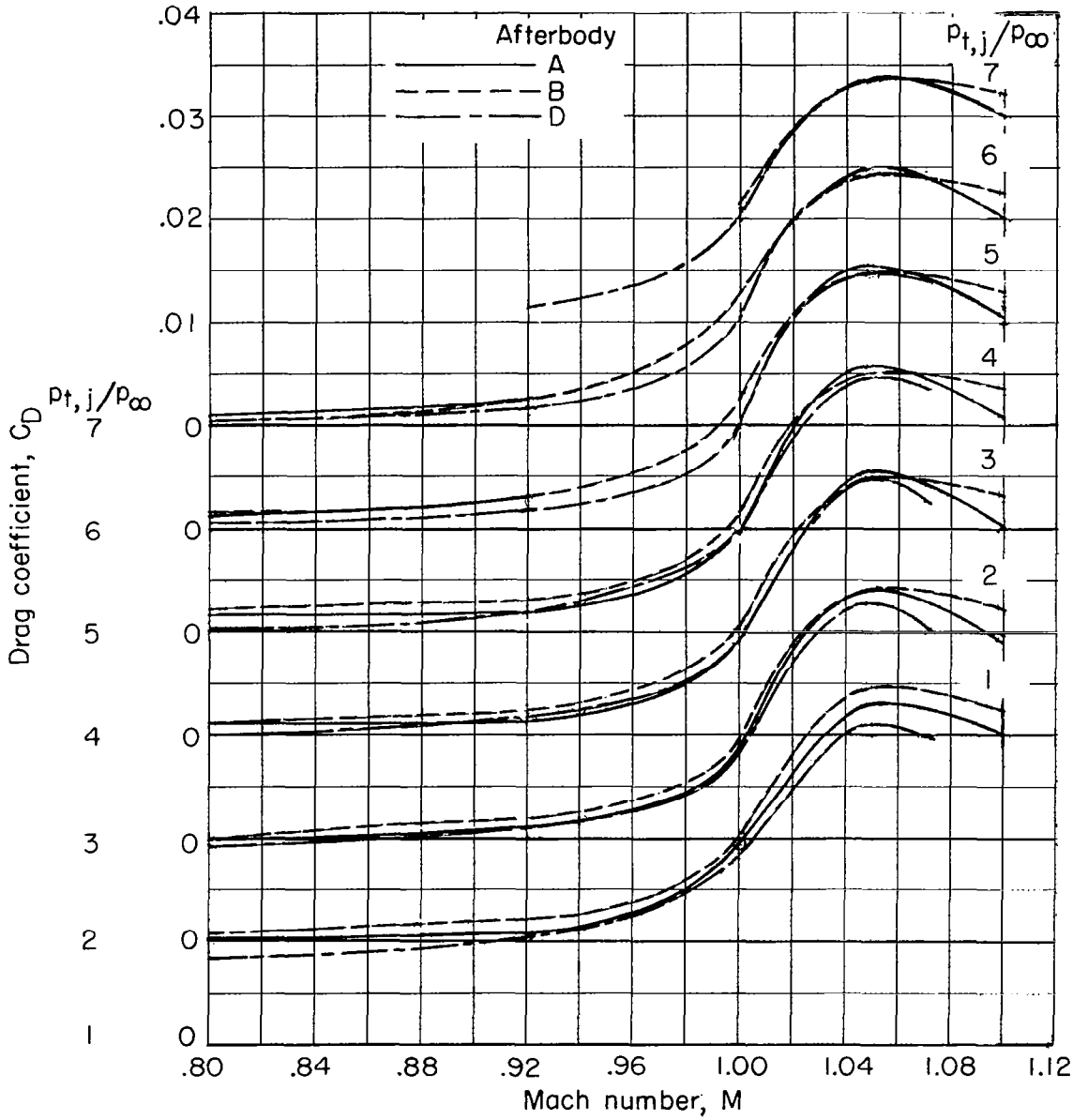

(a) Afterbodies A, B, and D.

Figure 11.- Effect of Mach number on drag coefficient at constant jet pressure ratios.

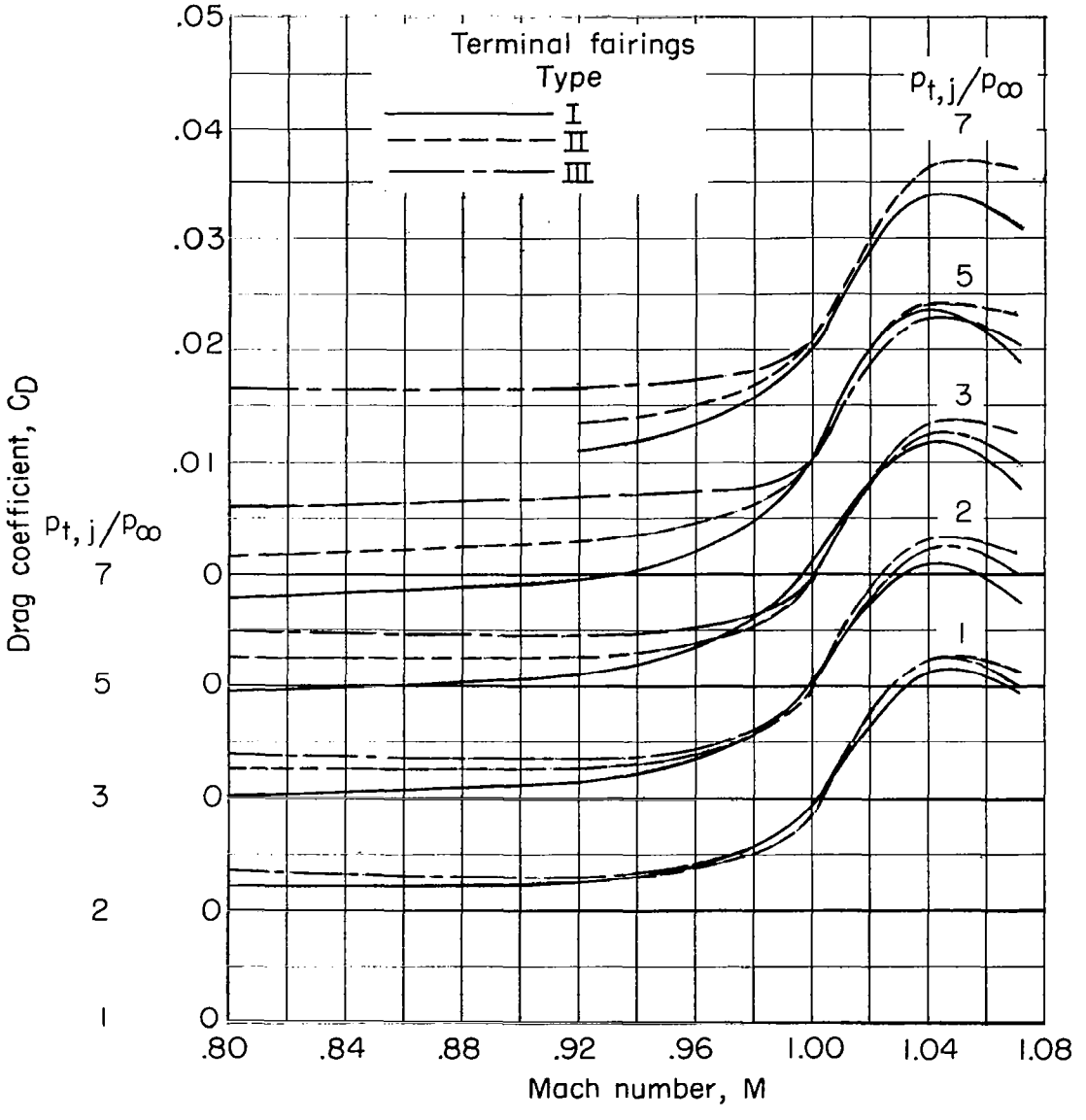

(b) Terminal fairings.

Figure 11.- Concluded.

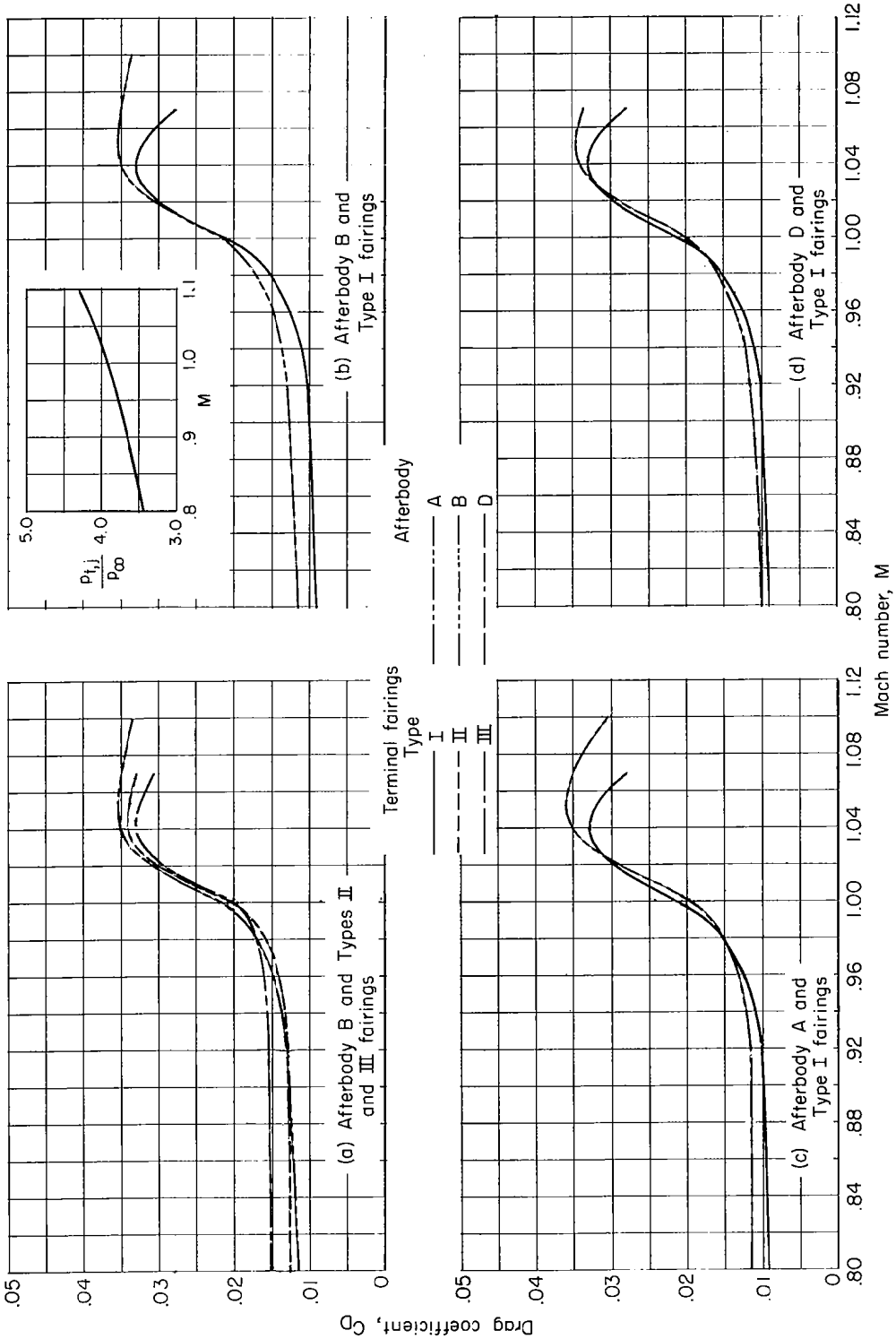

Figure 12.- Effect of Mach number on drag coefficient for a scheduled variation of jet pressure ratio.